Article

Neuron

Il10 Deficiency Rebalances Innate Immunity to Mitigate Alzheimer-Like Pathology

Highlights

- *Il10* deficiency promotes Alzheimer's β-amyloid clearance in *APP/PS1* mice
- *Il10* deficiency mitigates synaptic and cognitive deficits in *APP/PS1* mice
- Innate immunity is "rebalanced" in *Il10* deficient *APP/PS1* mouse brains
- Blocking IL-10 may be therapeutically relevant for Alzheimer's disease

Authors

Marie-Victoire Guillot-Sestier, Kevin R. Doty, ..., Kavon Rezai-Zadeh, Terrence Town

Correspondence

ttown@usc.edu

In Brief

In this issue, Guillot-Sestier et al. demonstrate that inhibiting IL-10 signaling, a key anti-inflammatory pathway, alters microglial activation in favor of cerebral Aβ phagocytosis. These results highlight that rebalancing cerebral innate immunity may be therapeutically relevant for Alzheimer's disease.

Accession Numbers

PRJNA219136

Guillot-Sestier et al., 2015, Neuron *85*, 534–548
February 4, 2015
http://dx.doi.org/10.1016/j.neuron.2014.12.068

CellPress

CellPress

Neuron
Article

Il10 Deficiency Rebalances Innate Immunity to Mitigate Alzheimer-Like Pathology

Marie-Victoire Guillot-Sestier,[1] Kevin R. Doty,[1] David Gate,[1] Javier Rodriguez, Jr.,[1] Brian P. Leung,[1] Kavon Rezai-Zadeh,[2] and Terrence Town[1,*]

[1]Zilkha Neurogenetic Institute, Department of Physiology & Biophysics, Keck School of Medicine of the University of Southern California, 1501 San Pablo Street, Los Angeles, CA 90089-2821, USA

[2]Pennington Biomedical Research Center, Louisiana State University, 6400 Perkins Road, Baton Rouge, LA 70808, USA

*Correspondence: ttown@usc.edu

http://dx.doi.org/10.1016/j.neuron.2014.12.068

SUMMARY

The impact of inflammation suppressor pathways on Alzheimer's disease (AD) evolution remains poorly understood. Human genetic evidence suggests involvement of the cardinal anti-inflammatory cytokine, interleukin-10 (*IL10*). We crossed the *APP/PS1* mouse model of cerebral amyloidosis with a mouse deficient in *Il10* (*APP/PS1*$^{+}$*Il10*$^{-/-}$). Quantitative in silico 3D modeling revealed activated Aβ phagocytic microglia in *APP/PS1*$^{+}$*Il10*$^{-/-}$ mice that restricted cerebral amyloidosis. Genome-wide RNA sequencing of *APP/PS1*$^{+}$*Il10*$^{-/-}$ brains showed selective modulation of innate immune genes that drive neuroinflammation. *Il10* deficiency preserved synaptic integrity and mitigated cognitive disturbance in *APP/PS1* mice. In vitro knockdown of microglial *Il10-Stat3* signaling endorsed Aβ phagocytosis, while exogenous IL-10 had the converse effect. *Il10* deficiency also partially overcame inhibition of microglial Aβ uptake by human Apolipoprotein E. Finally, the IL-10 signaling pathway was abnormally elevated in AD patient brains. Our results suggest that "rebalancing" innate immunity by blocking the IL-10 anti-inflammatory response may be therapeutically relevant for AD.

INTRODUCTION

Alzheimer's disease (AD), the most common form of dementia in the elderly, is characterized by a triad of pathological features: extracellular amyloid deposits predominantly composed of amyloid-β (Aβ) peptides, intracellular neurofibrillary tangles (NFTs) chiefly comprised of abnormally folded tau protein, and gliosis consisting of reactive microglia and astrocytes surrounding β-amyloid plaques. During the past century, intense focus has been directed toward studying production, aggregation, and spreading of β-amyloid plaques and subsequent neurodegeneration (Mucke and Selkoe, 2012). These studies have led to the conclusion that AD pathology is driven by an imbalance between Aβ production and clearance.

Indeed, autosomal-dominant forms of familial Alzheimer's disease (FAD) are principally linked to mutations affecting β-amyloid precursor protein (β-APP) or Presenilin 1 (PS1) function (De Strooper et al., 2012), leading to amyloidogenic processing of β-APP and accumulation of cerebral amyloid deposits. Nonetheless, the vast majority of patients have the sporadic form of the disease, which likely arises from a combination of poorly defined genetic and environmental risk factors. These factors do not necessarily affect β-APP proteolysis, and it has instead been suggested that dysregulated Aβ clearance—rather than production—is the etiologic driving force in sporadic AD (Mawuenyega et al., 2010). As the resident macrophages of the CNS, microglia are chiefly responsible for phagocytosis and clearance of cellular detritus. Furthermore, numerous studies have validated the ability of microglia to phagocytose Aβ peptides (Grathwohl et al., 2009; Herber et al., 2004; Wilcock et al., 2004; Wyss-Coray et al., 2001). However, mounting evidence suggests that microglia are dysfunctional in the AD brain (Lopes et al., 2008; Streit et al., 2009). While prolonged activation of brain inflammatory processes coordinated by the cerebral innate immune system is now accepted as an AD etiologic event (Wyss-Coray and Mucke, 2002), the role of anti-inflammatory pathways in Aβ clearance and AD pathobiology has been largely overlooked.

Inflammatory responses are kept under control by two key immunoregulatory cytokines: transforming growth factor-β (TGF-β) and interleukin-10 (IL-10) (Li and Flavell, 2008; Strle et al., 2001; Williams et al., 2004; Wyss-Coray and Mucke, 2002). Our laboratory has previously shown that blockade of anti-inflammatory TGF-β-Smad 2/3 signaling in innate immune cells mitigates cerebral amyloidosis and behavioral deficits in the Tg2576 mouse model (Town et al., 2008). These data suggest that the innate immune system can be harnessed to clear Aβ in the context of anti-inflammatory signaling inhibition. Remarkably, cerebral levels of IL-10 were increased in this scenario, in line with the elevated IL-10 signaling observed in reactive glia neighboring β-amyloid plaques in aged Tg2576 mice (Apelt and Schliebs, 2001). Also, a functional polymorphism within the *Il10* gene has been linked to increased risk of AD in some (Arosio et al., 2004; Lio et al., 2003; Ma et al., 2005; Vural et al., 2009), but not all, populations (Depboylu et al., 2003; Ramos et al., 2006; Scassellati et al., 2004).

IL-10 signaling induced by binding of IL-10 homodimer to its cognate receptor (IL-10R) leads to phosphorylation of associated Janus kinase 1 (Jak1) and downstream phosphorylation and

activation of signal transducer and activator of transcription 3 (STAT3). Phosphorylated STAT3 translocates to the nucleus, where it regulates transcription of downstream cytokines and inflammatory genes including *SOCS3* (Murray, 2006). To investigate putative involvement of the IL-10 pathway in AD-like pathology, we crossed the Tg(APP_{swe}, $PS1_{\Delta E9}$) mouse model of cerebral amyloidosis with animals deficient in *Il10*. Genetic disruption of *Il10* licensed Aβ phagocytosis by activated microglia and reduced Aβ load in *APP/PS1* mouse brains. Transcriptome analysis of brains from *APP/PS1*$^{+}$*Il10*$^{-/-}$ mice by RNA sequencing (RNAseq) revealed modulation of the inflammatory milieu, including select inflammatory and microglial regulatory genes. Finally, *Il10* deficiency partially rescued synaptic toxicity and behavioral impairment driven by the *APP/PS1* transgenes.

RESULTS

Deficiency in *Il10* Mitigates Cerebral Amyloidosis in *APP/PS1* Mice

To assess the role of *Il10* in AD-like pathology, we bred *Il10*$^{-/-}$ mice (Kühn et al., 1993) to Tg(APP_{swe},$PSEN1_{\Delta E9}$) animals (referred as *APP/PS1* mice in the present study) (Jankowsky et al., 2001, 2004). *APP/PS1*$^{+}$*Il10*$^{-/-}$ and *APP/PS1*$^{+}$*Il10*$^{+/-}$ mice were born at Mendelian ratios and exhibited no anatomical defects or premature death compared to *APP/PS1*$^{+}$*Il10*$^{+/+}$ mice. IL-10 levels measured in the plasma of 12-month-old mice followed an *Il10* allele-dependent expression pattern (pg of IL-10/ml of plasma: *APP/PS1*$^{+}$*Il10*$^{+/+}$, 19.0 ± 1.1 [n = 6], *APP/PS1*$^{+}$*Il10*$^{+/-}$ [n = 4], 10.8 ± 2.1**; *APP/PS1*$^{+}$*Il10*$^{-/-}$, 0.20 ± 0.04*** [n = 4]; **p > 0.01, ***p > 0.001 compared to *APP/PS1*$^{+}$*Il10*$^{+/+}$ mice by one-way ANOVA and Dunnett's post hoc test). At 12 to 13 months of age, *APP/PS1*$^{+}$*Il10*$^{-/-}$ mice manifested significantly reduced amyloid deposition in cingulate cortex (CC), entorhinal cortex (EC), and hippocampus (HC) as measured by thioflavin S histochemistry (Figures 1A and 1B; reductions versus *APP/PS1*$^{+}$*Il10*$^{+/+}$ mice: CC, 74%; EC, 78%; HC, 67%, ***p < 0.001; by one-way ANOVA and Dunnett's post hoc test). Furthermore, 4G8^{+} β-amyloid plaques were also significantly reduced in *APP/PS1*$^{+}$*Il10*$^{-/-}$ compared to *APP/PS1*$^{+}$*Il10*$^{+/+}$ animals (Figure 1C; CC, 67%; EC, 50%; HC, 70%, *p < 0.05, **p < 0.01, ***p < 0.001; one-way ANOVA and Dunnett's post hoc test). Aβ plaque morphometry was analyzed by blindly assigning plaques to one of three mutually exclusive categories based on maximum diameter. Surprisingly, *APP/PS1*$^{+}$*Il10*$^{-/-}$ mice had modest but statistically significant increases in abundance of small (<25 μm) plaques in the CC and EC versus *APP/PS1*$^{+}$*Il10*$^{+/+}$ animals (Figure S1A, *p < 0.05 by one-way ANOVA and Fisher's post hoc test). Yet, numbers of medium- (25–50 μm) and large-sized (>50 μm) plaques were significantly reduced by 48%–74% in the CC, and this effect trended toward significance in the EC and HC (Figures S1B and S1C, *p < 0.05; by one-way ANOVA and Fisher's post hoc test). In addition to Aβ plaques in brain parenchyma, 86% of AD patients deposit Aβ in cerebral blood vessels, known as cerebral amyloid angiopathy (CAA) (Ellis et al., 1996; Kanekiyo et al., 2012). *APP/PS1* mice also develop CAA, and this pathology was significantly reduced by 46%–68% in EC and HC (and trended toward significance in CC) in *APP/PS1*$^{+}$*Il10*$^{-/-}$ versus *APP/PS1*$^{+}$*Il10*$^{+/+}$ mice (Figure 1D, *p < 0.05, **p < 0.01; by one-way ANOVA and Dunnett's post hoc test). Interestingly, no evidence for *Il10* heterozygous advantage was found for Aβ deposits in brain parenchyma or cerebral vessels (Figures 1A–1D and S1, p > 0.05).

Biochemical analysis revealed striking reductions in both $A\beta_{1-40}$ and $A\beta_{1-42}$ abundance in brains of *APP/PS1*$^{+}$*Il10*$^{-/-}$ compared to *APP/PS1*$^{+}$*Il10*$^{+/+}$ mice. In the detergent-soluble fraction, $A\beta_{1-40}$ was reduced by 63% and $A\beta_{1-42}$ by 70% (Figures 1E and 1F, *p < 0.05, **p < 0.01; by one-way ANOVA and Dunnett's post hoc test). Additionally, after re-extraction of the detergent-insoluble pellet in the chaotropic agent, guanidine-HCl, $A\beta_{1-40}$ was lowered by 79% and $A\beta_{1-42}$, by 85% in *APP/PS1*$^{+}$*Il10*$^{-/-}$ versus *APP/PS1*$^{+}$*Il10*$^{+/+}$ mice (Figures 1G and 1H, *p < 0.05; by one-way ANOVA and Dunnett's post hoc test). Interestingly, detergent-soluble cerebral $A\beta_{1-40}$ and $A\beta_{1-42}$ abundance was decreased by 35%–42% in *APP/PS1*$^{+}$*Il10*$^{+/-}$ mice, although this trend did not reach statistical significance (Figures 1E and 1F, p > 0.05; by one-way ANOVA and Dunnett's post hoc test).

To rule out the possibility of an effect on cerebral amyloidosis due to altered APP_{Swe} or $PS1_{\Delta E9}$ transgene expression, western blot and quantitative real-time reverse transcriptase PCR (qPCR) analyses were performed on protein and RNA extracted from frontal cortex of all three groups of mice. No between-groups differences were found on PS1 or APP protein or mRNA levels (Figures 1I–1K). To determine if *Il10* deficiency altered APP metabolism, amyloidogenic C99 fragments were detected in frontal cortex brain extracts (n = 5 to 6 for each mouse group) by western blot but remained unmodified (quantitation of C99 band intensity normalized to holo-APP and β-actin: *APP/PS1*$^{+}$*Il10*$^{+/+}$, 99.5 ± 7.8; *APP/PS1*$^{+}$*Il10*$^{+/-}$, 96.8 ± 7.3; *APP/PS1*$^{+}$*Il10*$^{-/-}$, 87.9 ± 5.9, p > 0.05; by one-way ANOVA and Dunnett's post hoc test). Finally, to address the possibility of Aβ peptide efflux from brain to blood, we assayed plasma levels of $A\beta_{1-40}$ and $A\beta_{1-42}$ but did not detect significant differences (pg of $A\beta_{1-40}$/ml of plasma: *APP/PS1*$^{+}$*Il10*$^{+/+}$, 594.3 ± 92.8; *APP/PS1*$^{+}$*Il10*$^{+/-}$, 649.4 ± 90.3; *APP/PS1*$^{+}$*Il10*$^{-/-}$, 752.3 ± 55.4; pg of $A\beta_{1-42}$/mL of plasma: *APP/PS1*$^{+}$*Il10*$^{+/+}$, 220.2 ± 60.9; *APP/PS1*$^{+}$*Il10*$^{+/-}$, 372.8 ± 62.5; *APP/PS1*$^{+}$*Il10*$^{-/-}$, 294.4 ± 39.2, p > 0.05; by one-way ANOVA and Dunnett's post hoc test).

Il10 Deficiency Activates Innate Immunity in Brains of *APP/PS1* Mice

Within the CNS, IL-10 is mainly produced by astrocytes and microglia (Ledeboer et al., 2002), the latter being brain-resident innate immune cells that are centrally positioned to phagocytose and clear Aβ (Aguzzi et al., 2013; Guillot-Sestier and Town, 2013). To confirm the cellular source of cerebral IL-10 in our experimental animals, *Il10* mRNA levels were analyzed by qPCR in CD11b^{+} and CD11b^{-} cellular fractions isolated from brain single-cell suspensions (Figure S2A). The CD11b^{+} cell fraction highly expressed established microglial markers (i.e., *Iba1*, *Cx3cr1*, *Csf1r*, and *Itgb5*; Figure S2A) (Butovsky et al., 2014), while the CD11b^{-} cell fraction expressed astrocytic and neuronal markers (i.e., *S100b* and *Map2*). Interestingly, the CD11b^{+} fraction was largely enriched in *Il10r* mRNA compared to CD11b^{-} cells, and *Il10r* expression was strikingly increased in microglia from APP/PS1^{+} animals (Figure S2A). Finally, *Il10* mRNA levels were markedly increased in microglia from *APP/*

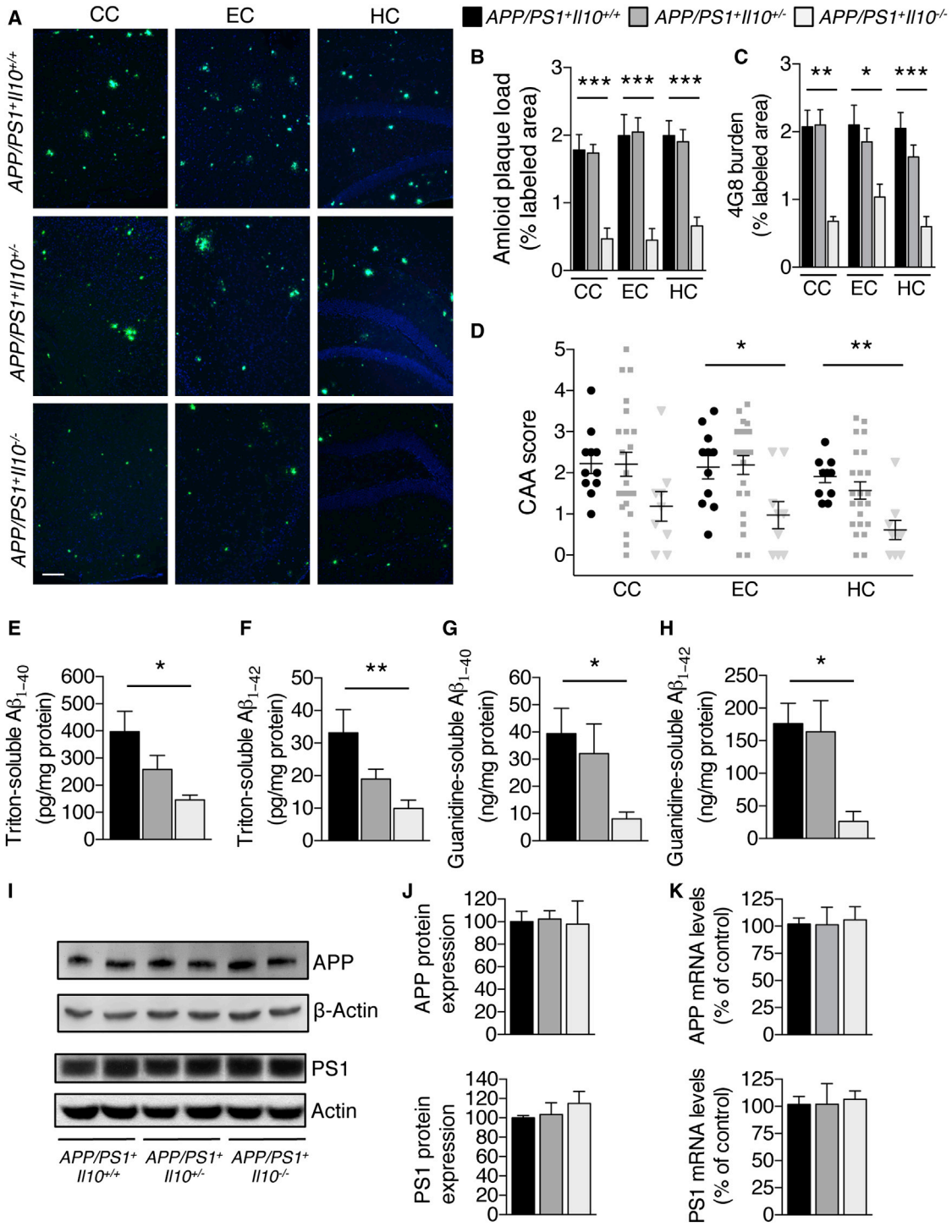

Figure 1. *Il10* Deficiency Reduces Cerebral Amyloidosis in *APP/PS1* Mice

(A) Representative micrographs of amyloid plaques labeled with thioflavin S from the CC, EC, and HC of *APP/PS1* mice homozygous, heterozygous, or completely deficient for *Il10*. Scale bar denotes 100 μm.

(B and C) Quantitation of thioflavin S (B) and 4G8 (C) labeling.

(D) Semiquantitative analysis of CAA severity (CAA score) from thioflavin S-labeled brain sections.

(E–H) ELISA analysis of frontal cortex detergent-soluble ([E] and [F]) or guanidine-HCl-extracted ([G] and [H]) $A\beta_{1-40}$ and $A\beta_{1-42}$ species from mice with the indicated genotypes. For (B)–(H), data are presented as mean ± SEM for *APP/PS1*$^{+}$*Il10*$^{+/+}$ (n = 10–18), *APP/PS1*$^{+}$*Il10*$^{+/-}$ (n = 9–24), and *APP/PS1*$^{+}$*Il10*$^{-/-}$ mice (n = 3–10); *p < 0.05, **p < 0.01, *and **p < 0.001.

(legend continued on next page)

PS1^{+}*Il10*$^{+/+}$ brains, suggesting that IL-10 is produced by CD11b^{+} microglia and likely participates in autocrine signaling via IL-10R in brains of *APP/PS1*$^{+}$ mice. To investigate the effect of *Il10* deficiency on neuroinflammation in response to Aβ deposition, coronal sections from 12- to 13-month-old mouse brains were immunostained for ionized calcium-binding receptor 1 (Iba1) (Ahmed et al., 2007), and data showed 54%–69% significantly increased signal in *APP/PS1*$^{+}$*Il10*$^{-/-}$ versus *APP/PS1*$^{+}$*Il10*$^{+/+}$ mice (Figure 2A, *p < 0.05, **p < 0.01; by one-way ANOVA and Dunnett's post hoc test). Interestingly, in non-transgenic animals, *Il10* deficiency did not modify Iba1^{+} immunoreactivity (% of labeled area: CC: *Il10*$^{+/+}$, 1.35 ± 0.16; *Il10*$^{-/-}$, 1.58 ± 0.19; EC: *Il10*$^{+/+}$, 1.03 ± 0.15; *Il10*$^{-/-}$, 1.44 ± 0.16; HC: *Il10*$^{+/+}$, 2.30 ± 0.43; *Il10*$^{-/-}$, 2.06 ± 0.23; n = 6 per genotype, by t test), indicating that *Il10* deficiency selectively modified microglial phenotype in the context of the *APP/PS1* transgenes. A similar pattern of statistically significant results (from 55%–64%) was observed for glial fibrillary acidic protein (GFAP)-reactive astrocytes in EC and HC (Figures 2B and 2C, *p < 0.05, ***p < 0.001; by one-way ANOVA and Dunnett's post hoc test). Remarkably, *APP/PS1*$^{+}$*Il10*$^{-/-}$ mice that still had remaining β-amyloid plaques demonstrated statistically significant 74%–143% increased CD11b^{+}-activated microglial burden (Townsend et al., 2005) in close vicinity of Aβ deposits in the CC, EC, and HC (Figures 2C and 2D, *p < 0.05, **p < 0.01; by one-way ANOVA and Dunnett's post hoc test). Further evidence of 59%–266% significantly increased microglial activation in *APP/PS1*$^{+}$*Il10*$^{-/-}$ mice came from CD45 immunostaining data (Figure 2E, *p < 0.05, ***p < 0.001; by one-way ANOVA and Dunnett's post hoc test) (Tan et al., 2000; Zhu et al., 2011). We did not observe histologic evidence of vascular cuffing or presence of round, non-process-bearing CD45 highly expressing (CD45^{hi}) mononuclear cells (Town et al., 2008), and flow cytometric analysis of single-cell suspensions isolated from *APP/PS1*$^{+}$*Il10*$^{+/+}$ versus *APP/PS1*$^{+}$*Il10*$^{-/-}$ brains showed no differences on abundance of CD45^{hi} or intermediate-expressing (CD45^{int}) populations (Figure S2B). Interestingly, amyloid plaques in *APP/PS1*$^{+}$*Il10*$^{-/-}$ mice appeared more diffuse than typical dense-cored plaques present in *APP/PS1*$^{+}$*Il10*$^{+/+}$ mice, and were accompanied by 50%–74% increased activated CD68^{+} microglia (Figures 2F and 2G, *p < 0.05; by one-way ANOVA and Dunnett's post hoc test). In addition, association of microglia with amyloid deposits was significantly enhanced by 34% in *APP/PS1*$^{+}$*Il10*$^{-/-}$ brains compared to *APP/PS1*$^{+}$*Il10*$^{+/+}$ littermates (p < 0,001; by t test).

Modified Neuroinflammatory Profile in *APP/PS1* Mice Deficient for *Il10*

To assess global transcriptional changes in brains of *APP/PS1* mice deficient in *Il10*, RNAseq was performed. Total brain mRNA was isolated from 12-month-old *APP/PS1*$^{+}$: *Il10*$^{+/+}$, *Il10*$^{+/-}$, *or Il10*$^{-/-}$ animals (n = 5 per group). Clustering of individual animal expression profiles resulted in segregation of the two homozygous populations, with heterozygous animals intermixed (Figure S3). Comparative expression of 14,800 detected RefSeq genes (normalized as RPKM; average per genotype) revealed expression changes that were *Il10* allele dependent (Figure 3A). Most genes remained unchanged in *APP/PS1*$^{+}$*Il10*$^{-/-}$ versus *APP/PS1*$^{+}$*Il10*$^{+/+}$ mice, with only 117 genes having greater than 2-fold differences. Cluster analysis of those 117 genes was performed, resulting in three distinct patterns: A, B, and C (Figure 3B). We further defined these groups as A1, A2, B, and C, where group A1 and A2 genes were decreased in *APP/PS1*$^{+}$*Il10*$^{-/-}$ mice and *APP/PS1*$^{+}$*Il10*$^{+/-}$ mice had an intermediate result; group B genes were only decreased in *APP/PS1*$^{+}$*Il10*$^{-/-}$ mice, and group C genes were increased in *APP/PS1*$^{+}$*Il10*$^{-/-}$ mice. When these genes were further interrogated for immune-related function(s), the majority of immune genes fell into groups A1 and A2 (Figure 3B). These genes, corresponding fold changes with associated statistical significance levels, and global function(s) in immune responses are presented in Figure 3C. Interestingly, expression of *Apoe* (a well-established genetic risk factor for late-onset AD) was reduced in *APP/PS1*$^{+}$*Il10*$^{-/-}$ compared to *APP/PS1*$^{+}$*Il10*$^{+/+}$ animals, validating microglial qPCR data (see Figure S2A). In general, immune genes with altered expression profiles were responsible for innate immune cell regulation, chemoattraction, Aβ interaction, and phagocytosis.

IL-10 Retards while *Il10* Deficiency Promotes Microglial Aβ Phagocytosis

Data described above suggested that *Il10* deficiency endorsed a beneficial form of innate immune activation that favored microglial β-amyloid clearance. To directly investigate the effects of IL-10 on microglial Aβ phagocytosis, primary cultures of microglia were established from *Il10*$^{+/+}$ or *Il10*$^{-/-}$ mice, and Aβ$_{1-42}$ phagocytosis was evaluated. Remarkably, ELISA measurement of Aβ$_{1-42}$ intracellular content showed recombinant IL-10 treatment to significantly decrease preaggregated Aβ$_{1-42}$ uptake by 41% in *Il10*$^{+/+}$ and 62% in *Il10*$^{-/-}$ mouse primary microglia (Figure 4A, *Il10*$^{+/+}$, †p = 0.06 and *Il10*$^{-/-}$, ***p < 0.001; by one-way ANOVA and Sidak's post hoc test), and a similar pattern of results was observed in a rat microglial cell line (data not shown). Treatment with recombinant IL-10 also (1) reduced phagolysosomal CD68 labeling by 49% (Figures S4A and S4B, *p < 0.05; by t test), (2) diminished intracellular Aβ$_{1-42}$-cy3 signal by 46% (Figure S4C, *p < 0.05; by t test), and (3) induced STAT3 translocation to the nucleus (Figures S4D and S4E, **p < 0.01; by t test). These data show that IL-10 treatment shifts microglial activation away from Aβ phagocytosis via increasing activation of STAT3.

In a reciprocal set of experiments, Aβ$_{1-42}$ uptake was increased by 60% in *Il10*$^{-/-}$ primary microglia (Figure 4A, *Il10*$^{+/+}$ versus *Il10*$^{-/-}$, *p < 0.05; by one-way ANOVA and Sidak's

(I) Western blots of human (h) APP or hPS1 levels in frontal cortex homogenates of *APP/PS1* mice with the indicated genotypes. β-actin is shown as a loading control.

(J) Quantitation of hAPP or hPS1 protein levels in frontal cortex homogenates from *APP/PS1* mice of the indicated genotypes. Expression levels are normalized to β-actin. Data are represented as mean ± SEM for n = 6 samples for each group, with *APP/PS1*$^{+}$*Il10*$^{+/+}$ signal normalized to 100%; non-significant.

(K) qPCR analysis of APP and PS1 mRNA levels in frontal cortex from mice with the indicated genotypes. The mRNA levels are normalized to *Hprt*, and data are represented as mean ± SEM for n = 6 per group; non-significant. See also Figure S1.

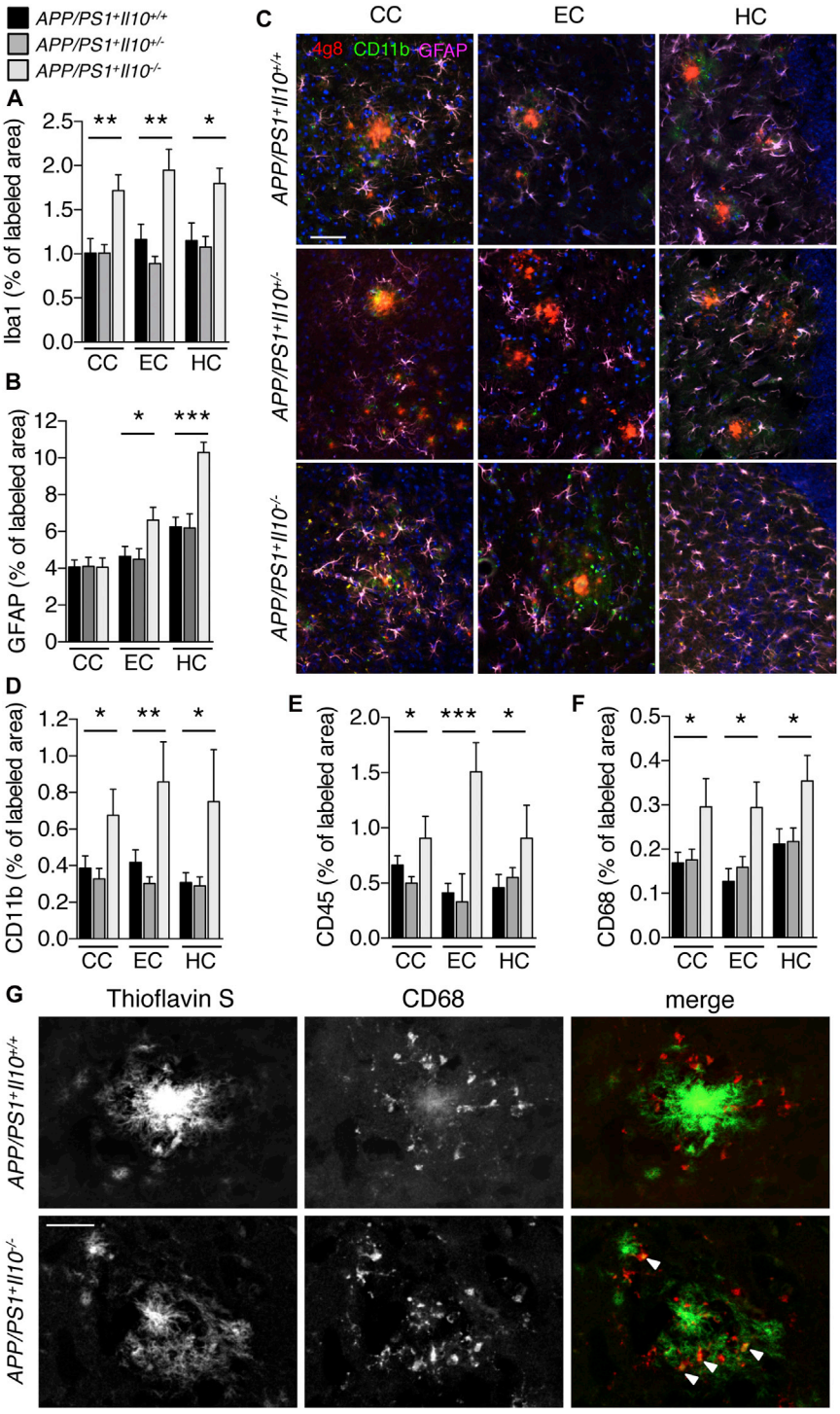

Figure 2. *Il10* Deficient *APP/PS1* Mice Activate Cerebral Innate Immunity

(A–F) Microgliosis and astrogliosis were quantified in coronal sections labeled with Iba1 (A), GFAP (B), CD11b (D), CD45 (E), or CD68 (F) antibodies in mice with the indicated genotypes. Data are represented as mean ± SEM for *APP/PS1*$^{+}$*Il10*$^{+/+}$ (n = 8–13), *APP/PS1*$^{+}$*Il10*$^{+/-}$ (n = 8–16), and *APP/PS1*$^{+}$*Il10*$^{-/-}$ mice (n = 3–10); *p < 0.05, **p < 0.01, and ***p < 0.001.

(C) Representative micrographs of CC, EC, and HC from *APP/PS1* mice homozygous, heterozygous, or completely deficient for *Il10*. Amyloid plaques were labeled using 4G8 antibody, and CD11b^{+} microglia or GFAP^{+} astrocytes were found associated with β-amyloid deposits. Scale bar denotes 50 μm.

(G) Representative microphotographs are shown of β-amyloid plaque morphology in cortex of *APP/PS1*$^{+}$*Il10*$^{-/-}$ versus *APP/PS1*$^{+}$*Il10*$^{+/+}$ mice. Amyloid plaques are labeled with thioflavin S while phagocytic microglia are marked by CD68 antibody. White arrows represent CD68^{+} cells colocalized with amyloid deposits. Scale bar denotes 20 μm. See also Figure S2.

post hoc test). To determine if *Stat3* knockdown could phenocopy the effect of *Il10* deletion on microglial Aβ phagocytosis, we used a mouse microglial cell line (N9) that responded similarly to mouse primary microglia in terms of IL-10-dependent reduction of Aβ phagocytosis (Figure S4F, *p < 0.05; by t test). Three independent *Stat3* knockdown microglial N9 lines were generated via *shStat3* lentiviral infection, and STAT3 expression was validated by immunocytochemistry and western blot (Figures S4G and S4H). Strikingly, reduced STAT3 nuclear translocation occurred with increased $A\beta_{1-42}$-cy3 within CD68^{+} lysosomes (Figure S4I) in the same manner as *Il10* deletion.

To further investigate this effect, morphology and Aβ phagocytic aptitude of *Il10*$^{+/+}$ versus *Il10*$^{-/-}$ primary microglia were evaluated by live cell imaging. Twenty-four hours after transfection with a Lamp1-GFP construct, cells were challenged with $A\beta_{1-42}$-cy3 to follow $A\beta_{1-42}$ uptake into Lamp1^{+} phagolysosomes. Representative images from Movies S1 and S2 are shown in Figure 4B. Interestingly, $A\beta_{1-42}$-cy3 was encapsulated within Lamp1^{+} structures in both *Il10*$^{+/+}$ and *Il10*$^{-/-}$ microglia; however, Aβ-containing phagolysosomes were enlarged in *Il10*$^{-/-}$ microglia (Figure 4B; see white arrows and Movies S1 and S2).

Strikingly, a similar pattern of results was observed in vivo. *APP/PS1*$^{+}$ mice presented Iba1^{+} microglia containing 4G8^{+} Aβ encapsulated within Lamp1^{+} (Figures 4C and 4D) and CD68^{+} (Figure S4J) phagolysosomes. Yet, *APP/PS1*$^{+}$*Il10*$^{-/-}$ brains had demonstrably increased abundance of Iba1^{+} microglia that costained for Lamp1^{+} lysosomes and for 4G8^{+} Aβ (Figures 4C and 4D). Importantly, phagolysosomes within Iba1^{+} cells were increased by 92% in the cortex and 140% in HC of *APP/PS1*$^{+}$*Il10*$^{-/-}$ versus *APP/PS1*$^{+}$*Il10*$^{+/+}$ mice (Figure 4E, *p < 0.05, **p < 0.01; by t test). Analysis of plaque-associated microglia

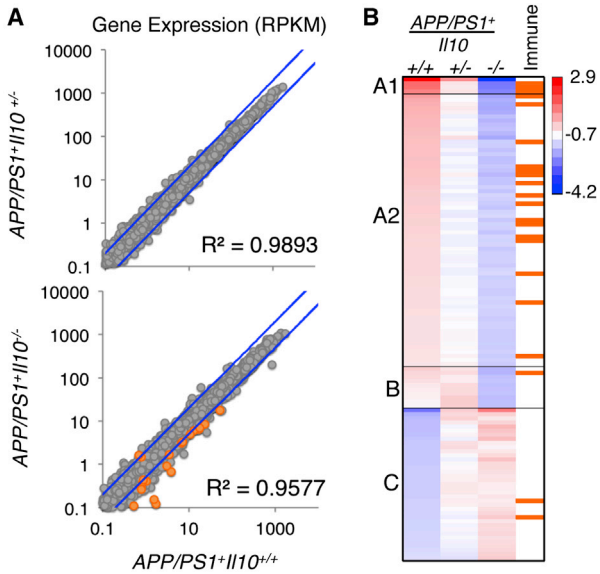

C

Gene	Log_2FC	FDR	Group	Role
Clec7a	-3.9	$1x10^{-04}$	A1	Phagocytosis/ Chemoattraction
Itgax	-3.7	$6x10^{-04}$	A1	
Ccl6	-2.6	$3x10^{-04}$	A2	
Fcer1g	-1.3	$3x10^{-05}$	A2	
Cxcl10	-2.5	$8x10^{-03}$	A2	
Ccl3	-3.3	$1x10^{-04}$	A1	Pro-inflammatory
Lyz1	-1.7	$3x10^{-04}$	A2	Innate Immune Regulation
Lyz2	-1.4	$5x10^{-03}$	A2	
Tyrobp	-1.5	$1x10^{-04}$	A2	
Trem2	-1.4	$2x10^{-04}$	A2	
Mpeg1	-1.1	$8x10^{-04}$	A2	
Tlr2	-1.4	$3x10^{-03}$	A2	Amyloid-β interaction
C4b	-1.1	$1x10^{-03}$	A2	
C3ar1	-1.0	$4x10^{-03}$	A2	
Apoe	-0.6	$4x10^{-05}$	A2	
Cd48	-1.3	$3x10^{-03}$	A2	T cell activation/ chemoattraction
Cxcl16	-1.1	$4x10^{-03}$	A2	
Tnfrsf18	1.2	$8x10^{-04}$	C	
Fcgr2b	-1.0	$1x10^{-03}$	A2	B cell co-receptor
Egr4	-1.0	$3x10^{-03}$	A2	Transcription factors
Atf3	-1.6	$3x10^{-04}$	B	
Ifit3	-1.1	$3x10^{-04}$	A2	Inhibitor cell migration/ proliferation/virus replication
Thpo	0.9	$9x10^{-03}$	C	Megakaryocytopoeisis/ platelet production

Figure 3. Transcriptome Analysis of Brains from *APP/PS1* Mice Deficient in *Il10*

(A) Scatterplot of the average expression per gene (RPKM) of *APP/PS1*$^{+}$*Il10*$^{+/+}$ (n = 5) plotted against *APP/PS1*$^{+}$*Il10*$^{+/-}$ (n = 5) or *APP/PS1*$^{+}$*Il10*$^{-/-}$ mice (n = 5). The blue line represents a 2-fold change.

(B) A heatmap of k means cluster analysis of log_2-transformed expression (RPKM) is shown for 117 genes with 2-fold or greater change. Genes that are immune related (as reported by the KEGG database) are indicated in orange.

(C) A table of immune- and inflammation-related genes identified from the heatmap with log_2 (fold change) of *APP/PS1*$^{+}$*Il10*$^{+/+}$ versus *APP/PS1*$^{+}$*Il10*$^{-/-}$ mice is shown, and false discovery rate is calculated by the edgeR package in Bioconductor. See also Figure S3.

revealed an increased proportion of cells containing phagolysosome-encapsulated amyloid in *Il10*-deficient animals (Figure 4F; cortex, 62%; HC, 60%, ***p < 0.001; by t test). Finally, the total amount of 4G8^{+} Aβ loaded within Lamp1^{+} phagolysosomes was significantly augmented in *APP/PS1*$^{+}$*Il10*$^{-/-}$ versus *APP/PS1*$^{+}$*Il10*$^{+/+}$ brains (Figure 4G; cortex, 148%; HC, 110%, *p < 0.05, **p < 0.01; by t test). Altogether, our results demonstrate that *Il10* deficiency enhances microglial amyloid phagocytic function in *APP/PS1* mice.

We previously observed by brain RNAseq (Figure 3) and microglial qPCR (Figure S2A) that *Apoe* expression was reduced in *APP/PS1*$^{+}$*Il10*$^{-/-}$ mice. To determine if human ApoE isoforms (E2, E3, and E4) acted as molecular chaperones to bind Aβ and alter microglial phagocytosis, we preincubated Cy3-labeled (Figure 4H) or unlabeled (Figure 4I) human recombinant $Aβ_{1–42}$ with human recombinant ApoE2, ApoE3, or ApoE4. *Il10*$^{+/+}$ and *Il10*$^{-/-}$ primary microglial cultures were then treated with this mixture. Human ApoE drastically reduced Aβ uptake by microglia in an isoform-specific manner (E4>E3>E2), mirroring the well-established ApoE-human AD risk relationship (Figure 4H). This was confirmed by ELISA quantitation of Aβ uptake in a parallel set of experiments using unlabeled Aβ (Figure 4I, **p < 0.01, ***p < 0.001; by one-way ANOVA and post hoc t test). Strikingly, human ApoE isoform-dependent reduction of microglial Aβ phagocytosis was significantly rescued by *Il10* deficiency in the case of ApoE3.

Il10 Deficiency Preserves Synaptic Integrity in *APP/PS1* Mice

A key challenge for immunomodulatory strategies that promote cerebral amyloid clearance is avoidance of bystander neuronal injury due to neuroinflammation (Guillot-Sestier and Town, 2013; Town et al., 2005). To determine whether synaptic health was impacted by *Il10* deficiency in *APP/PS1* mice, coronal brain sections from 12-month-old mice were stained with an antibody directed against synaptophysin. As predicted, synaptophysin puncta density was reduced by 37%–40% in *APP/PS1*$^{+}$*Il10*$^{+/+}$ versus *APP/PS1*$^{-}$*Il10*$^{+/+}$ littermates, both in HC and in cerebral cortex (Figures 5A–5C; *p < 0.05, **p < 0.01, by one-way ANOVA and Dunnett's post hoc test). Strikingly, however, *APP/PS1*$^{+}$*Il10*$^{-/-}$ mice had hippocampal and cortical synaptophysin labeling density that was restored to that of *APP/PS1*$^{-}$ littermates (Figures 5A–5C). Western blot analysis of cortical protein extracts confirmed our immunohistochemical observations (Figure 5D), and densitometric analysis disclosed reduced synaptophysin abundance in brains of *APP/PS1*$^{+}$*Il10*$^{+/+}$ and *APP/PS1*$^{+}$*Il10*$^{+/-}$ mice compared to non-transgenic controls (*APP/PS1*$^{-}$*Il10*$^{+/+}$, n = 6, normalized to 1 versus *APP/PS1*$^{+}$*Il10*$^{+/+}$, 0.52 ± 0.20*, n = 6; and *APP/PS1*$^{-}$*Il10*$^{+/-}$, 1.07 ± 0.33, n = 6 versus *APP/PS1*$^{+}$*Il10*$^{+/-}$, 0.65 ± 0.33*, n = 8; *p < 0.05 by one-way ANOVA and Sidak's post hoc test). Remarkably, *Il10* deficiency in *APP/PS1*$^{+}$ mice normalized synaptophysin abundance to non-transgenic animals (*APP/PS1*$^{+}$*Il10*$^{-/-}$, 0.72 ± 0.12, n = 5 versus *APP/PS1*$^{-}$*Il10*$^{-/-}$, 0.97 ± 0.30, n = 3; not significantly different by one-way ANOVA and Sidak's post hoc test). The beneficial effect of *Il10* loss on synaptophysin abundance was *APP/PS1* transgene dependent, because synaptophysin levels were not affected in *Il10* heterozygotes or *Il10*-deficient mice that lacked the *APP/PS1* transgenes (Figure 5D; p > 0.05, by one-way ANOVA and Dunnett's post hoc test).

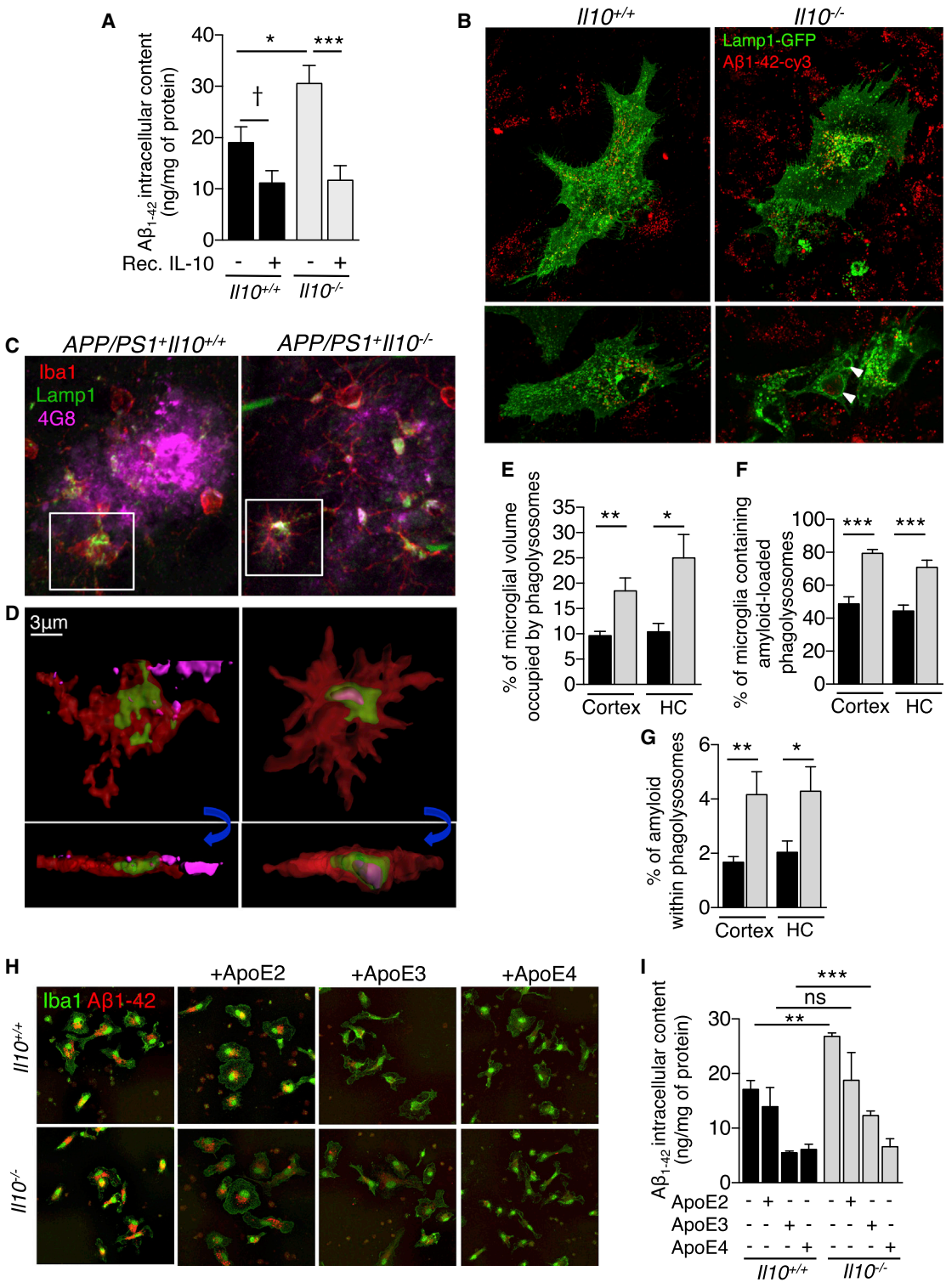

Figure 4. *Il10* Deficiency Increases Microglial β-Amyloid Phagocytosis

(A) ELISA analysis of $A\beta_{1-42}$ intracellular content in cultured $Il10^{+/+}$ or $Il10^{-/-}$ mouse primary microglia. Cultures were treated for 2 hr with recombinant IL-10 before challenge with human synthetic $A\beta_{1-42}$ microaggregates for 6 hr. Data are presented as mean ± SEM of four independent experiments carried out in duplicate; †p = 0.06, *p < 0.05, and ***p < 0.001.

(B) Representative microphotographs of Lamp1-GFP-transfected primary cultures of microglia ($Il10^{+/+}$ or $Il10^{-/-}$) challenged with $A\beta_{1-42}$-cy3 microaggregates. White arrows designate enlarged $Lamp1^{+}$ phagolysosomes containing $A\beta_{1-42}$-cy3 in $Il10^{-/-}$ microglia.

(legend continued on next page)

Deficiency in *Il10* Mitigates *APP/PS1* Transgene-Associated Behavioral Impairment

To evaluate functional consequences of preserved synaptic health in *APP/PS1*$^{+}$*Il10*$^{-/-}$ mice, all six groups of littermates were cognitively evaluated. Prior to behavioral testing, mice were subjected to neurological screening to assess auditory, visual, and olfactory acuity and response to a tactile stimulus. Additionally, coordination, balance, and grip strength were tested. Mice performed equally well for each of the neurological screening tests (data not shown), and so all animals were included in subsequent behavioral assays. Locomotion and spontaneous activity were tested in an open field. Yet, no significant differences between any of the six groups were observed when considering rearing or time spent in the center of the field (Figure S5A), indicating that subsequent behavioral results were not distorted by variation in anxiety between genotypes. However, when considering fine movements (i.e., grooming, exploration on four limbs, and sniffing) and total activity, *APP/PS1*$^{+}$*Il10*$^{+/+}$ mice were hyperactive versus controls, a behavioral phenotype that may result from cortical and hippocampal injury leading to disinhibition (Town et al., 2008). Strikingly, *APP/PS1*$^{+}$*Il10*$^{-/-}$ mice had complete mitigation of hyperactivity (Figures 6A and S5A; † $p < 0.1$, *$p < 0.05$, ****$p < 0.0001$; by one-way ANOVA and Fisher's LSD post hoc test).

Next, learning and episodic memory were assessed in the novel object recognition test, which is dependent on hippocampal and cortical function (Hammond et al., 2004). If mice remember a previously encountered object compared to a novel object, they tend to preferentially explore the new object more than the familiar one. As expected, after a 1 hr retention period, *APP/PS1*$^{+}$*Il10*$^{+/+}$ mice trended toward lower preference for the novel object than controls (Figure 6B; † $p = 0.07$; by one-way ANOVA and Fisher's LSD post hoc test). Strikingly, defective novel object recognition was completely remediated by *Il10* deficiency, and partial amelioration of this behavioral defect was observed in *APP/PS1*$^{+}$*Il10*$^{+/-}$ mice (Figure 6B). A similar trend of results occurred after 24 hr of retention (Figure S5B). Importantly, neither short-term (1 hr) nor long-term (24 hr) novel object memory were affected by *Il10* deficiency in non-transgenic controls (Figure 6B and Figure S5B; $p > 0.05$, by one-way ANOVA and Fisher's LSD or Sidak's post hoc tests, respectively).

Spatial working memory was evaluated by spontaneous alternation in the Y-maze (Deacon et al., 2002). Similar to the open-field test, *APP/PS1*$^{+}$*Il10*$^{+/+}$ mice were hyperactive compared to control littermates, as operationalized by total number of arm entries. Again, this behavioral phenotype was completely mitigated by *Il10* deficiency (Figure 6C, *$p \leq 0.05$; by one-way ANOVA and Fisher's LSD post hoc test). As expected, *APP/PS1*$^{+}$*Il10*$^{+/+}$ mouse percentage spontaneous alternation trended toward less frequent than controls, and *Il10* deficiency did not modify this effect (Figure 6D, † $p = 0.07$; by one-way ANOVA and Fisher's LSD post hoc test). As an important control, deficiency in *Il10* did not alter spontaneous alternation in control littermates lacking the *APP/PS1* transgene (Figure 6D, $p > 0.05$; by one-way ANOVA and Fisher's LSD post hoc test).

Finally, mice were tested for HC-dependent spatial reference learning and memory in the Barnes maze (O'Leary and Brown, 2009). During the training phase, all of the mouse groups demonstrated reduced latency to escape with successive acquisition trials, with the exception of *APP/PS1*$^{+}$*Il10*$^{-/-}$ mice, which completed training in two distinct phases. During the six first trials, acquisition of the escape hole location was faster than the other groups, but *APP/PS1*$^{+}$*Il10*$^{-/-}$ mice spent more time searching the escape box during the rest of the training (Figure S5C, *$p < 0.05$; by one-way ANOVA and Fisher's LSD post hoc test). In the probe trial, latency to escape the maze was increased in *APP/PS1*$^{+}$*Il10*$^{+/+}$ mice compared to non-transgenic controls. However, complete *Il10* deficiency did not significantly restore *APP/PS1* behavioral deficit in this task. Surprisingly though, *APP/PS1*$^{+}$*Il10*$^{+/-}$ mice performed significantly better than *APP/PS1*$^{+}$*Il10*$^{+/+}$ animals in the probe trial (Figure S5D, *$p < 0.05$; by one-way ANOVA and Fisher's LSD post hoc test). During the reversal phase of the test, no differences in acquisition of the new escape box location were observed between the six groups (Figure S5E, $p < 0.05$; by one-way ANOVA and Fisher's LSD post hoc test). No statistically significant gender differences were found for any of the behavioral paradigms, and so males and females were considered together in all behavioral analyses.

IL-10 Signaling Is Elevated in AD Patient Brains

Finally, we sought to evaluate IL-10 signaling in postmortem samples from AD patient brains versus age-matched, non-demented controls. Hippocampal sections were stained for IL-10 receptor alpha chain (IL-10Rα) and microtubule-associated protein 2 (MAP2, a neuronal marker). Interestingly, IL10Rα expression was elevated in AD compared to control brains, and some of these signals could be found colocalized with MAP2^{+} neurons (Figures 7A, see white arrowheads, and 7B;

(C) Representative microphotographs of amyloid deposits in cortex of *APP/PS1*$^{+}$*Il10*$^{-/-}$ versus *APP/PS1*$^{+}$*Il10*$^{+/+}$ mice. Amyloid deposits are labeled with 4G8 and microglia, with Iba1 and Lamp1.

(D) 3D reconstruction from confocal image stacks showing 4G8^{+} Aβ encapsulated within Lamp1^{+} structures in Iba1^{+} microglia present in brains of *APP/PS1*$^{+}$*Il10*$^{-/-}$ versus *APP/PS1*$^{+}$*Il10*$^{+/+}$ mice. Blue arrows indicate rotation of insets in the Z-plane to show presence of Aβ within phagolysosomes.

(E–G) Quantitation of microglial volume occupied by Lamp1^{+} phagolysosomes (E), percent of Iba1^{+} microglia containing amyloid-loaded phagolysosomes (F), or 4G8^{+} amyloid encapsulated in phagolysosomes (G) in the EC and HC of mice with the indicated genotypes. Data are represented as mean ± SEM for *APP/PS1*$^{+}$*Il10*$^{+/+}$ (n = 4) or *APP/PS1*$^{+}$*Il10*$^{-/-}$ (n = 5) mice; *$p < 0.05$, **$p < 0.01$, ***$p < 0.001$.

(H) Representative microphotographs of Iba1^{+} primary cultures of microglia (*Il10*$^{+/+}$ or *Il10*$^{-/-}$) challenged with $A\beta_{1-42}$-cy3 microaggregates preincubated with human recombinant ApoE2, ApoE3, or ApoE4.

(I) ELISA analysis of $A\beta_{1-42}$ intracellular content in cultured mouse primary microglia (*Il10*$^{+/+}$ or *Il10*$^{-/-}$). Cells were treated for 6 hr with human synthetic $A\beta_{1-42}$ preaggregated in presence of recombinant ApoE2, ApoE3, or ApoE4. Data are presented as mean ± SEM of two independent experiments carried out in duplicate; **$p < 0.01$; ***$p < 0.001$. See also Figure S4 and Movies S1 and S2.

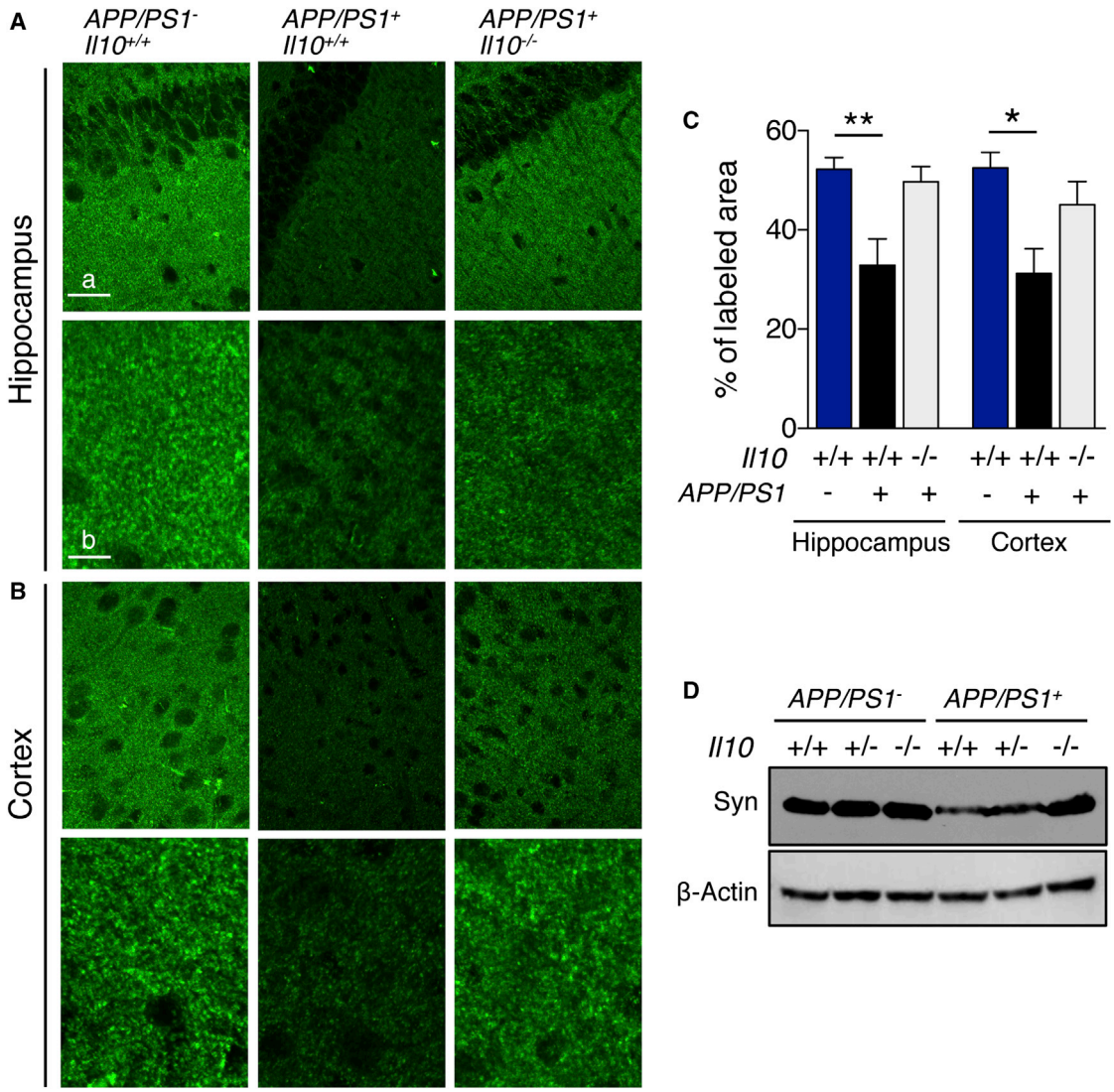

Figure 5. Preservation of Synaptic Integrity in *Il10* Deficient *APP/PS1* Mice

(A and B) Representative microphotographs of synaptophysin labeling in HC (A) or cortex (B) of mice with the indicated genotypes. Lower panels are 3.5× higher magnification of the upper images. Scale bars denote (a) 87 μm or (b) 25 μm.

(C) Quantitation of synaptophysin labeling in HC and cortex is shown as mean ± SEM (n = 4 per group); *p < 0.05; **p < 0.01.

(D) Western blot of synaptophysin levels in frontal cortex homogenates of mice with the indicated genotypes. β-actin served as a loading control.

**p < 0.01; by student's t test). Furthermore, phospho-Jak1, a key downstream effector kinase of the IL-10 pathway, was elevated in AD brains in close proximity to thioflavin S^+ amyloid plaques (Figures 7C and 7D, *p < 0.05; by student's t test). Western blot analyses of hippocampal protein extracts from a separate cohort confirmed our immunohistochemical observations, with densitometry disclosing increases of 6.5-fold in IL10Rα (Figure 7E, *p < 0.05), 2.3-fold in Jak1 (Figure 7F, †p = 0.09), 2.6-fold in phospho-Jak1 (Figure 7G, *p < 0.05), 4.2-fold in STAT3 (Figure 7H, *p < 0.05), 1.6-fold in phospho-STAT3 (Figure 7I, †p = 0.1), and 1.9-fold in SOCS3 (Figure 7J, †p = 0.07) abundance (all by student's t test). Taken together, these data indicate elevated IL-10 signaling in AD patient versus age-matched control brains. Interestingly, we also observed increased *Il10* and *Il10r* mRNA levels in microglia isolated from brains of APP/$PS1^+$ mice (Figure S2A).

DISCUSSION

While once regarded as epiphenomenon, the impact of the cerebral innate immune response on AD pathology has become a topic of intense interest (Gandy and Heppner, 2013; Guillot-Sestier and Town, 2013; Weitz and Town, 2012). This has prompted the need for a deeper understanding of which innate immune pathways are deregulated in the context of the disease. While proinflammatory cytokines have received attention in this regard, the concept that dysregulated anti-inflammatory cytokines may be deleterious in AD has been largely overlooked. While several

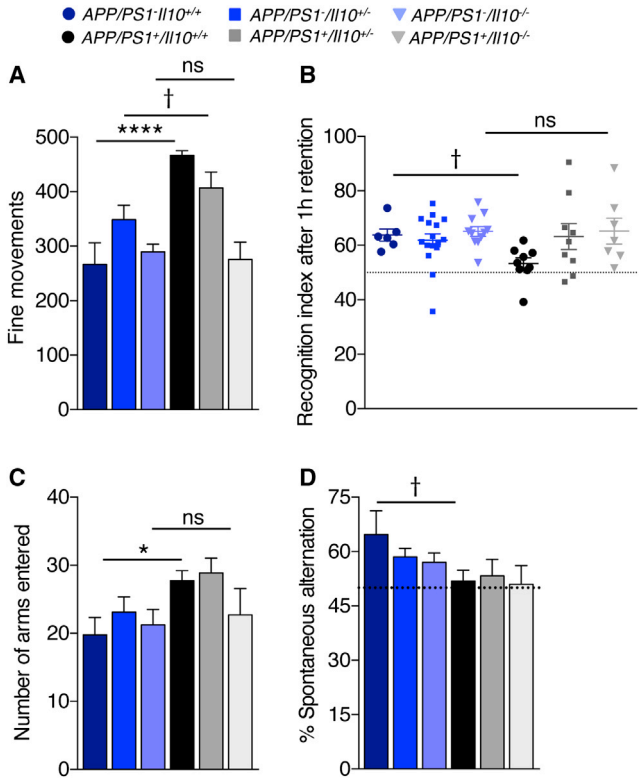

Figure 6. *Il10* Deficiency Partially Restores Cognitive Function in *APP/PS1* Mice

(A) Spontaneous activity was tested in the open field over a 30 min period. Bars represent fine movements of the mice.

(B) Evaluation of episodic memory in the novel object recognition test after 1 hr of retention. Plots represent the recognition index.

(C and D) Determination of spontaneous alternation in the Y-maze. Bars represent number of arms entered (C) or percent spontaneous alternation (D). Data are represented as mean ± SEM for $Il10^{+/+}$ (n = 5 to 6), $Il10^{+/-}$ (n = 15 to 16), $Il10^{-/-}$ (n = 8–11), $APP/PS1^{+}Il10^{+/+}$ (n = 8–10), $APP/PS1^{+}Il10^{+/-}$ (n = 8 to 9), and $APP/PS1^{+}Il10^{-/-}$ mice (n = 7) compared to $APP/PS1^{-}$ groups; †$p \leq 0.1$, *$p \leq 0.05$, and ****$p < 0.0001$. See also Figure S5.

studies have shown that *Il10* polymorphism is associated with late onset AD (Arosio et al., 2004; Lio et al., 2003; Ma et al., 2005; Vural et al., 2009), almost nothing is known regarding the putative role of IL-10 in evolution of disease pathology.

To address this knowledge gap, we generated *APP/PS1* mice deficient for *Il10* and evaluated AD-like pathology and cognitive impairment. Results showed strikingly reduced cerebral amyloid pathology in these animals, and remaining plaques were associated with activated microglia. Interestingly, plaques in $APP/PS1^{+}Il10^{-/-}$ mice had a "moth-eaten" morphology, similar to observations made in brains of AD patients or *APP* transgenic mice after $A\beta_{1\text{-}42}$ immunization (Bard et al., 2000; Nicoll et al., 2003, 2006; Schenk et al., 1999; Zotova et al., 2011). Importantly, $CD68^{+}$ phagocytic microglial cells were observed invading moth-eaten plaques in $APP/PS1^{+}Il10^{-/-}$ brains. Recently, Krabbe and colleagues showed that microglial cells fail to reduce Aβ burden in transgenic mouse models of AD due to impaired mobility and phagocytic capacity (Krabbe et al., 2013). Microglial "paralysis" may be owed to increasing Aβ burden with disease progression, as shown by others in vitro and in vivo (Korotzer et al., 1993; Krabbe et al., 2013; Michelucci et al., 2009). Alternatively, it has been hypothesized that microglial senescence in the aging brain could be responsible for reduced capacity of these cells to clear cerebral amyloid (Lopes et al., 2008; Miller and Streit, 2007; Streit et al., 2009). The results we report here show that stimulation of microglia by recombinant IL-10 induces nuclear translocation of the downstream signal transducer STAT3 and reduces Aβ phagocytosis, whereas *Il10* deficiency or *Stat3* knockdown increases Aβ uptake by cultured microglia. Additionally, *Il10* deficiency increases microglial activation and promotes Aβ uptake into $Lamp1^{+}$ and $CD68^{+}$ phagolysosomes in vivo. In this regard, *Il10* deficiency in *APP/PS1* mice seems to restore physiologic ability to phagocytose Aβ. These findings dovetail with previous studies from our laboratory and others, showing that induction of a proinflammatory activation state endorses cerebral amyloid clearance (Chakrabarty et al., 2010a, 2010b, 2011; Shaftel et al., 2007; Town et al., 2008). We did not observe histological evidence of brain-infiltrating peripheral mononuclear phagocytes in $APP/PS1^{+}Il10^{-/-}$ mice (i.e., vascular cuffing or presence of round, non-process-bearing leukocytes) as we previously reported in a different innate immune paradigm (Town et al., 2008). Furthermore, *Il10* deficiency did not modify abundance of $CD45^{hi}$ or $CD45^{int}$ mononuclear phagocytes in $APP/PS1^{+}Il10^{+/+}$ versus $APP/PS1^{+}Il10^{-/-}$ brains, suggesting that brain-resident microglia are likely the major population responsible for amyloid clearance. However, direct experiments aimed at firmly delineating the role of peripheral versus central phagocytes in clearance of Aβ are warranted.

The study of global transcriptome changes in brains of *APP/PS1* mice via RNAseq demonstrates that *Il10* deficiency modifies cerebral innate immunity. During the analysis, we considered classical markers for M2-like (TGF-β, Ym-1, and Fizz) and M1-like (TNF-α, IL-1β, and IL-6) innate immune activation states. However, we did not detect differential expression of these targets. Yet, *Clec7a* expression was strongly decreased in $APP/PS1^{+}Il10^{-/-}$ mice, suggesting polarization of microglial activation away from the M2 state. Depending on the type of stimulation, microglia demonstrate remarkable plasticity and often respond with a mixed activation phenotype (Ghassabeh et al., 2006; Town et al., 2005); therefore, we have previously suggested that M1 or M2 define boundaries of a more broad microglial activation continuum (Town et al., 2005). Nonetheless, our data reveal global changes in genes that regulate innate immune activation, inflammation, and phagocytosis. Interestingly, genes upregulated in brains of patients with late onset AD such as *Tyrobp*, *Trem2*, and *C4b* (Brouwers et al., 2012; McGeer et al., 1989; Zhang et al., 2013) were decreased in brains of *Il10*-deficient *APP/PS1* mice. Along similar lines, previous studies have shown that TLR2 and C4b bind Aβ and trigger microglial activation (Richard et al., 2008) and Aβ fibril formation (Sjölander et al., 2012; Trouw et al., 2008), and $APP/PS1^{+}Il10^{-/-}$ brains had decreased expression of both genes. Strikingly, Chakrabarty and coworkers have demonstrated that adeno-associated viral expression of *Il10* in brains of APP transgenic mice leads to age-dependent upregulation of *Cxcl10*, *Tlr2*, *C4b*, and *C3ar1* transcripts (Chakrabarty et al., 2015). These global gene

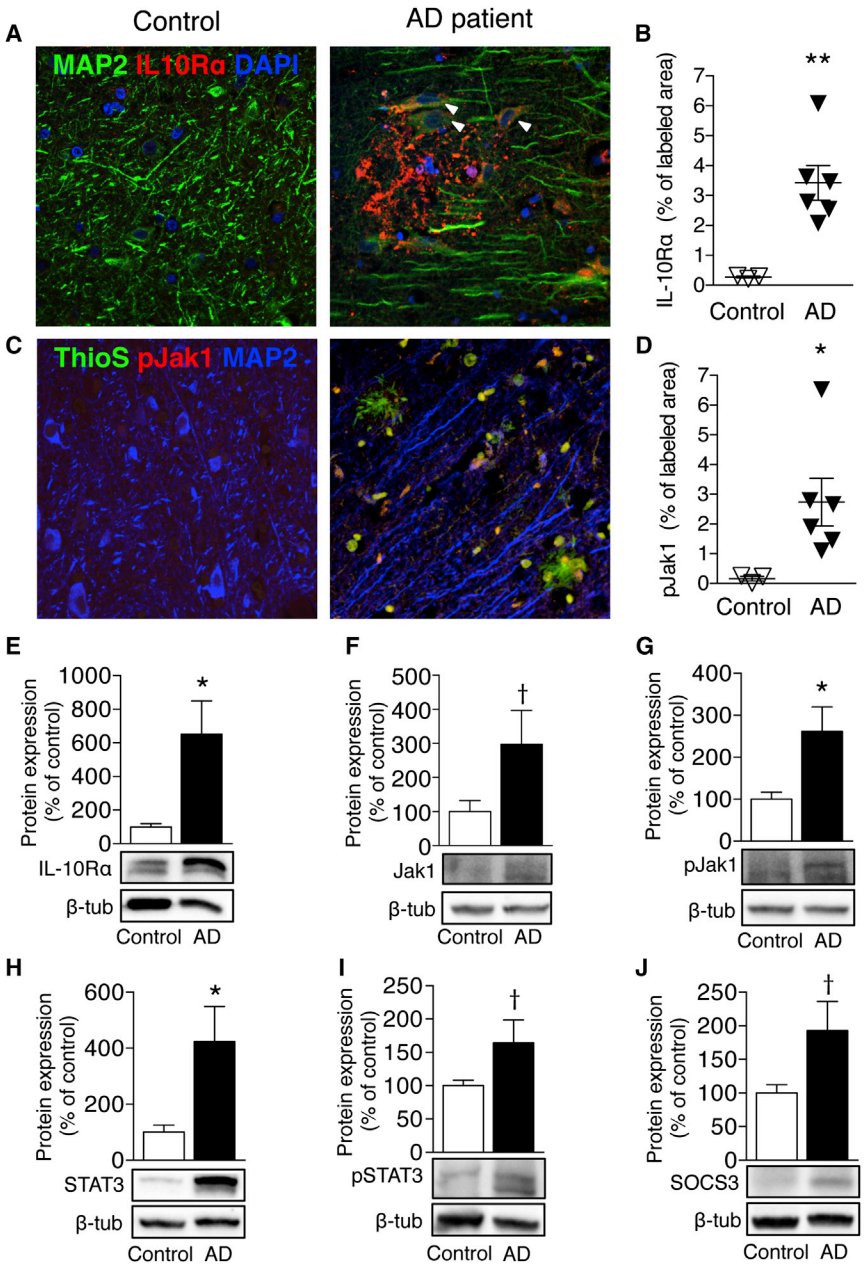

Figure 7. IL-10 Signaling Is Elevated in AD Patient Brains

(A) Representative microphotographs of IL10Rα (red) and MAP-2 (green) labeling in hippocampal sections of AD patients and age-matched, non-demented control subjects.

(B) Quantitation of IL10Rα immunoreactivity in AD (n = 6) and control (n = 3) brain sections; data are presented as mean ± SEM of labeled area for three optical sections per subject; **p < 0.01.

(C) Representative microphotographs of thioflavin S^+ amyloid plaques (green), MAP-2 (blue), and phospho-Jak1 (pJak1, red) signals in hippocampal sections of AD patients and age-matched, non-demented controls.

(D) Quantitation of pJak1 levels in AD (n = 6) and control (n = 3) brain sections; data are presented as mean ± SEM of labeled area for 3 optical sections per subject; *p < 0.05.

(E–J) Quantification and representative western blots of IL10Rα (E), Jak1 (F), pJak1 (G), STAT3 (H), pSTAT3 (I), and SOCS3 (J) in hippocampal homogenates of AD patients and age-matched, non-demented controls. Expression levels are normalized to β-tubulin. Data are represented as mean ± SEM for controls (n = 6) and AD (n = 8) patients; †p < 0.1; *p < 0.05.

expression results corroborate our data showing that *Il10* deficiency restores microglial functionality that is compromised in *APP/PS1* transgenic mice. Of particular interest, *Apoe* expression was reduced in *APP/PS1*$^{+}$*Il10*$^{-/-}$ mice as shown by brain RNAseq ($log_2FC = -0.6$, FDR = 4×10^{-5}) and by microglial qPCR. In vitro, recombinant human ApoE3 and ApoE4 drastically impaired Aβ uptake by microglia, while ApoE2 had no effect, mirroring the well-established ApoE-human AD risk relationship. Strikingly, *Il10* deficiency partially rescued human ApoE3-associated reduction of Aβ uptake compared to *Il10*$^{+/+}$ microglia, but was unable to recover the deleterious effect of human ApoE4. Again, this tracks well with ApoE4 increased risk for human AD.

But does remodeling of cerebral amyloid in *APP/PS1*$^{+}$*Il10*$^{-/-}$ mice come at the cost of bystander injury to neurons? This question is especially pertinent because we and others have shown that gliosis can potentially be toxic to neurons in the context of AD (Maezawa et al., 2011; Meda et al., 1995; Tan et al., 1999). Given changes in immune gene expression profile associated with *Il10* deficiency and mitigation of cerebral amyloid load, we examined synaptic health in *APP/PS1*$^{+}$*Il10*$^{-/-}$ animals. Synaptophysin density was reduced in HC and cortex of *APP/PS1* mice compared to non-transgenic controls, as reported in transgenic mouse models of cerebral amyloidosis and in AD patients (Buttini et al., 2005; Imbimbo et al., 2010; Tampellini et al., 2010; Ubhi et al., 2010). Interestingly, synaptophysin loss in *APP/PS1* mice was almost completely restored by *Il10* deficiency, indicating that innate immune activation associated with amyloid clearance in *APP/PS1*$^{+}$*Il10*$^{-/-}$ mice preserved synaptic integrity.

Behavioral analyses were performed to determine whether maintenance of synaptic health in *APP/PS1*$^{+}$*Il10*$^{-/-}$ mice translated to better cognitive function. Importantly, in non-transgenic control groups, *Il10* deficiency did not alter anxiety, learning, or memory. On the other hand, *APP/PS1* mice were hyperactive, likely resulting from disinhibition associated with hippocampal or cortical damage (Hsiao et al., 1996; Town et al., 2008). Additionally, novel object recognition and spatial working

memory were defective in *APP/PS1* mice, as previously reported (Hooijmans et al., 2009; O'Leary and Brown, 2009; Webster et al., 2013). Most importantly, *Il10* deficiency mitigated *APP/PS1* transgene-associated hyperactivity in both the open-field and Y-maze tasks, and both short- and long-term novel object recognition were completely restored. However, spatial memory deficits were not rescued in *APP/PS1*$^{+}$*Il10*$^{-/-}$ mice, although spatial reference memory was completely mitigated in *APP/PS1*$^{+}$*Il10*$^{+/-}$ animals. This latter finding is significant because eventual clinical therapeutic targeting of IL-10 would likely never achieve 100% inhibition. These results indicate that *Il10* deficiency mitigates a subset of defective cognitive function in *APP/PS1* mice.

To address the possibility that we were simply studying iatrogenic events not related to human AD, we investigated IL-10 signaling in AD patients versus cognitively healthy, age-matched controls. Data showed that expression of the cognate IL-10 receptor, IL10Rα, was elevated in AD patient brains compared to age-matched, non-demented individuals. Phosphorylated (activated) Jak1 was correspondingly increased in cells surrounding amyloid plaques in AD specimens, and protein levels of IL-10 receptor and downstream effectors were elevated in AD hippocampal homogenates. Collectively, these results indicate abnormally increased IL-10 signaling in AD patient brains. These results corroborate and extend the observations of other groups that reported increased levels of IL-10 in serum and brain extracts from AD patients (Angelopoulos et al., 2008; Culpan et al., 2006; Loewenbrueck et al., 2010). Furthermore, we noted that *Il10* as well as *IL10r* mRNA levels were increased in microglia extracted from *APP/PS1*$^{+}$*Il10*$^{+/+}$ mouse brains, suggesting an autocrine signaling mechanism associated with increased cerebral amyloidosis, a finding that is in line with the IL-10 immunoreactive cells observed in close vicinity to β-amyloid deposits in 13-month-old Tg2576 mice (Apelt and Schliebs, 2001). Since we show that recombinant IL-10 treatment inhibits Aβ uptake by cultured microglia, elevated IL-10 signaling in AD patient brains and *APP/PS1*$^{+}$ mice may hinder the physiological ability of microglia to phagocytose and clear cerebral amyloid.

Altogether, our findings show that genetic blockade of *Il10* promotes a beneficial form of cerebral innate immunity. *Il10* blockade enables cerebral Aβ clearance via two independent mechanisms: (1) reducing IL-10/STAT3 signaling to enhance microglial phagocytic activity and (2) decreasing microglial *Apoe* expression, thereby mitigating ApoE-Aβ binding and detrimental reduction of Aβ phagocytosis. Importantly, our data are consistent with recent results showing that forced *Il10* expression in brains of *APP* transgenic mice leads to increased Aβ accumulation and worsening of behavioral deficits (Chakrabarty et al., 2015). Therefore, modulating IL-10 signaling alters the microglial activation footprint and Aβ phagocytosis. Collectively, these results suggest that rebalancing cerebral innate immunity and promoting beneficial neuroinflammation may be more efficacious than generalized anti-inflammatory therapy for AD.

EXPERIMENTAL PROCEDURES

Please see Supplemental Experimental Procedures for detailed methods on immunochemistry, primary microglia isolation, flow cytometry, cell culture, transfection and viral infection, live cell imaging, Aβ uptake quantitation, western blots, ELISA and MSD technology, RNAseq and qPCR, and behavioral experiments.

Human Brain Samples

Frozen human brain tissue used for western blotting was obtained from the Alzheimer's Disease Research Center (ADRC, NIA AG05142) Neuropathology Core (three female and five male AD patient hippocampal samples, 51–100 years old, and four female and two male control hippocampal samples, 74–93 years old). For IHC, paraffin-embedded 10-μm-thick sections from the HC of six AD patients (three females and three males, 84–87 years old) and three age-matched non-demented control subjects were obtained from Dr. Serguei Bannykh, director of the Department of Neuropathology at Cedars-Sinai Medical Center.

Animals

Tg(*APP*$_{swe}$,*PSEN1*$_{\Delta E9}$) transgenic mice (referred to as *APP/PS1* in this report; B6.Cg-Tg(APPswe,PSEN1dE9)85Dbo/Mmjax MMRRC, stock #034832) (Jankowsky et al., 2004) were bred with *Il10* knockout mice (Kühn et al., 1993) (B6.129P2-*Il10*^{tm1Cgn}/J, stock #002251). Both mouse strains are on the C57BL/6 background and were obtained from the Jackson Laboratory. All mice were housed under standard conditions with free access to food and water, and all animal experiments were approved by the University of Southern California Institutional Animal Care and Use Committee and performed in strict accordance with National Institutes of Health guidelines and recommendations from the Association for Assessment and Accreditation of Laboratory Animal Care International.

Tissue Handling

Mice were perfused with ice-cold PBS and brains were extracted and quartered according to our previously published methods (Tan et al., 2002; Town et al., 2008). The anterior two quarters were snap-frozen and posterior quarters were fixed in 4% paraformaldehyde overnight for subsequent agarose or paraffin embedding.

3D Reconstruction of Confocal Images

Confocal image stacks (acquired at 60× magnification) of amyloid deposits-associated microglia were converted to 3D images with the surface-rendering feature of Imaris BitPlane software (version 7.6.1).

RNAseq Gene Expression Analysis

Strand-specific libraries were generated with 1 μg of input RNA using the TruSeq Stranded mRNA Sample Prep Kit (Illumina) on an Illumnia HiSeq 2000. Gene classes were generated with Cluster3 by applying k means clustering to mean-centered $\log_2$(RPKM) expression values (de Hoon et al., 2004). Classification of a gene as immune-related was based on KEGG pathway annotation (www.genome.jp/kegg).

Behavioral Analyses

Behavioral experiments were conducted with age-matched littermates from 12 to 13 months of age, inclusive of the following six genotypes: *Il10*$^{+/+}$, *Il10*$^{+/-}$, *Il10*$^{-/-}$, *APP/PS1*$^{+}$*Il10*$^{+/+}$, *APP/PS1*$^{+}$*Il10*$^{+/-}$, or *APP/PS1*$^{+}$*Il10*$^{-/-}$. All experiments were done blind with respect to the genotype of the mice. After neurological screening, behavioral tests were conducted in increasing order of difficulty and stress ranging from open field testing, novel object recognition, the Y-maze task, and the Barnes maze. For each test independently, mice that did not perform the exercise were excluded from the analysis.

Statistical Analysis

GraphPad Prism software, version 6.0, was used for all statistics. Multiple group comparisons were performed by one-way analysis of variance followed by Dunnett's, Sidak's, or Fisher's LSD post hoc tests. Otherwise, Student's t test was performed. For each behavioral test, possible gender differences within each group were statistically evaluated by analysis of variance, followed by Sidak's multiple comparison test. In all cases, $p \leq 0.05$ was considered to be statistically significant. All data are presented as means ± SEM.

ACCESSION NUMBERS

The RNAseq data have been deposited under NCBI BioProject accession number PRJNA219136.

SUPPLEMENTAL INFORMATION

Supplemental Information includes five figures, two movies, and Supplemental Experimental Procedures and can be found with this article online at http://dx.doi.org/10.1016/j.neuron.2014.12.068.

AUTHOR CONTRIBUTIONS

M.V.G.S. performed primary microglia, qPCR, and behavioral experiments. K.R.D. performed RNAseq and shRNA lentiviral infections. M.V.G.S., D.G., K.R.D., K.R.Z., B.P.L, and T.T. performed immunostaining, western blots, and ELISA. M.V.G.S. and D.G. performed in vivo 3D modeling and quantitations, live cell imaging, and flow cytometry. J.R. maintained the mouse colony. K.R.D. and D.G. equally contributed to this work. M.V.G.S. and T.T. wrote the manuscript. T.T. directed the project.

ACKNOWLEDGMENTS

We thank Dr. Serguei Bannykh for human brain sections, Dr. Jean-Philippe Vit for assistance with behavioral testing (Cedars Sinai Medical Center, Los Angeles), Dr. Carol A. Miller from the Alzheimer's Disease Research Center for frozen human brain tissue (University of Southern California, Los Angeles), and Dr. Eliezer Masliah (University of California, San Diego) for assistance with the synaptophysin immunostaining protocol. We sincerely thank Dr. Tara Weitz (USC Zilkha Neurgenetic Institute, Los Angeles), Drs. Todd Golde, and Paramita Chakrabarty (Center for Translational Research in Neurodegenerative Disease, University of Florida, Gainesville, FL, USA) and Dr. Pritam Das (Mayo Clinic, Jacksonville) for helpful discussion. We thank Alexander Vesling for technical help with primary microglial cells, and we thank the UCLA Neuroscience Genomics Core (Los Angeles) for assistance with RNAseq. D.G. is supported by an NIH National Research Service Award (1F31NS083339-01A1). This work was supported by the National Institute on Aging (5R00AG029726-04 and 3R00AG029726-04S1, to T.T.), the National Institute on Neurologic Disorders and Stroke (1R01NS076794-01, to T.T.), an Alzheimer's Association Zenith Fellows Award (ZEN-10-174633, to T.T.), and an American Federation of Aging Research/Ellison Medical Foundation Julie Martin Mid-Career Award in Aging Research (M11472, to T.T.). Finally, we are grateful for startup funds from the Zilkha Neurogenetic Institute, which made this work possible.

Received: September 17, 2013
Revised: November 28, 2014
Accepted: December 24, 2014
Published: January 22, 2015

REFERENCES

Aguzzi, A., Barres, B.A., and Bennett, M.L. (2013). Microglia: scapegoat, saboteur, or something else? Science *339*, 156–161.

Ahmed, Z., Shaw, G., Sharma, V.P., Yang, C., McGowan, E., and Dickson, D.W. (2007). Actin-binding proteins coronin-1a and IBA-1 are effective microglial markers for immunohistochemistry. J. Histochem. Cytochem. *55*, 687–700.

Angelopoulos, P., Agouridaki, H., Vaiopoulos, H., Siskou, E., Doutsou, K., Costa, V., and Baloyiannis, S.I. (2008). Cytokines in Alzheimer's disease and vascular dementia. Int. J. Neurosci. *118*, 1659–1672.

Apelt, J., and Schliebs, R. (2001). Beta-amyloid-induced glial expression of both pro- and anti-inflammatory cytokines in cerebral cortex of aged transgenic Tg2576 mice with Alzheimer plaque pathology. Brain Res. *894*, 21–30.

Arosio, B., Trabattoni, D., Galimberti, L., Bucciarelli, P., Fasano, F., Calabresi, C., Cazzullo, C.L., Vergani, C., Annoni, G., and Clerici, M. (2004). Interleukin-10 and interleukin-6 gene polymorphisms as risk factors for Alzheimer's disease. Neurobiol. Aging *25*, 1009–1015.

Bard, F., Cannon, C., Barbour, R., Burke, R.L., Games, D., Grajeda, H., Guido, T., Hu, K., Huang, J., Johnson-Wood, K., et al. (2000). Peripherally administered antibodies against amyloid beta-peptide enter the central nervous system and reduce pathology in a mouse model of Alzheimer disease. Nat. Med. *6*, 916–919.

Brouwers, N., Van Cauwenberghe, C., Engelborghs, S., Lambert, J.C., Bettens, K., Le Bastard, N., Pasquier, F., Montoya, A.G., Peeters, K., Mattheijssens, M., et al. (2012). Alzheimer risk associated with a copy number variation in the complement receptor 1 increasing C3b/C4b binding sites. Mol. Psychiatry *17*, 223–233.

Butovsky, O., Jedrychowski, M.P., Moore, C.S., Cialic, R., Lanser, A.J., Gabriely, G., Koeglsperger, T., Dake, B., Wu, P.M., Doykan, C.E., et al. (2014). Identification of a unique TGF-β-dependent molecular and functional signature in microglia. Nat. Neurosci. *17*, 131–143.

Buttini, M., Masliah, E., Barbour, R., Grajeda, H., Motter, R., Johnson-Wood, K., Khan, K., Seubert, P., Freedman, S., Schenk, D., and Games, D. (2005). Beta-amyloid immunotherapy prevents synaptic degeneration in a mouse model of Alzheimer's disease. J. Neurosci. *25*, 9096–9101.

Chakrabarty, P., Ceballos-Diaz, C., Beccard, A., Janus, C., Dickson, D., Golde, T.E., and Das, P. (2010a). IFN-gamma promotes complement expression and attenuates amyloid plaque deposition in amyloid beta precursor protein transgenic mice. J. Immunol. *184*, 5333–5343.

Chakrabarty, P., Jansen-West, K., Beccard, A., Ceballos-Diaz, C., Levites, Y., Verbeeck, C., Zubair, A.C., Dickson, D., Golde, T.E., and Das, P. (2010b). Massive gliosis induced by interleukin-6 suppresses Abeta deposition in vivo: evidence against inflammation as a driving force for amyloid deposition. FASEB J. *24*, 548–559.

Chakrabarty, P., Herring, A., Ceballos-Diaz, C., Das, P., and Golde, T.E. (2011). Hippocampal expression of murine TNFα results in attenuation of amyloid deposition in vivo. Mol. Neurodegener. *6*, 16.

Chakrabarty, P., Li, A., Ceballos-Diaz, C., Eddy, J.A., Funk, C.C., Moore, B., DiNunno, N., Rosario, A.M., Cruz, P.E., Verbeeck, C., et al. (2015). IL-10 Alters Immunoproteostasis in APP mice, Increasing Plaque Burden and Worsening Cognitive Behavior. Neuron *85*, this issue, 519–533.

Culpan, D., Prince, J.A., Matthews, S., Palmer, L., Hughes, A., Love, S., Kehoe, P.G., and Wilcock, G.K. (2006). Neither sequence variation in the IL-10 gene promoter nor presence of IL-10 protein in the cerebral cortex is associated with Alzheimer's disease. Neurosci. Lett. *408*, 141–145.

de Hoon, M.J., Imoto, S., Nolan, J., and Miyano, S. (2004). Open source clustering software. Bioinformatics *20*, 1453–1454.

De Strooper, B., Iwatsubo, T., and Wolfe, M.S. (2012). Presenilins and γ-secretase: structure, function, and role in Alzheimer Disease. Cold Spring Harb Perspect Med *2*, a006304.

Deacon, R.M., Bannerman, D.M., Kirby, B.P., Croucher, A., and Rawlins, J.N. (2002). Effects of cytotoxic hippocampal lesions in mice on a cognitive test battery. Behav. Brain Res. *133*, 57–68.

Depboylu, C., Du, Y., Müller, U., Kurz, A., Zimmer, R., Riemenschneider, M., Gasser, T., Oertel, W.H., Klockgether, T., and Dodel, R.C. (2003). Lack of association of interleukin-10 promoter region polymorphisms with Alzheimer's disease. Neurosci. Lett. *342*, 132–134.

Ellis, R.J., Olichney, J.M., Thal, L.J., Mirra, S.S., Morris, J.C., Beekly, D., and Heyman, A. (1996). Cerebral amyloid angiopathy in the brains of patients with Alzheimer's disease: the CERAD experience, Part XV. Neurology *46*, 1592–1596.

Gandy, S., and Heppner, F.L. (2013). Microglia as dynamic and essential components of the amyloid hypothesis. Neuron *78*, 575–577.

Ghassabeh, G.H., De Baetselier, P., Brys, L., Noël, W., Van Ginderachter, J.A., Meerschaut, S., Beschin, A., Brombacher, F., and Raes, G. (2006). Identification of a common gene signature for type II cytokine-associated myeloid cells elicited in vivo in different pathologic conditions. Blood *108*, 575–583.

Grathwohl, S.A., Kälin, R.E., Bolmont, T., Prokop, S., Winkelmann, G., Kaeser, S.A., Odenthal, J., Radde, R., Eldh, T., Gandy, S., et al. (2009). Formation and maintenance of Alzheimer's disease beta-amyloid plaques in the absence of microglia. Nat. Neurosci. *12*, 1361–1363.

Guillot-Sestier, M.V., and Town, T. (2013). Innate immunity in Alzheimer's disease: a complex affair. CNS Neurol. Disord. Drug Targets *12*, 593–607.

Hammond, R.S., Tull, L.E., and Stackman, R.W. (2004). On the delay-dependent involvement of the hippocampus in object recognition memory. Neurobiol. Learn. Mem. *82*, 26–34.

Herber, D.L., Roth, L.M., Wilson, D., Wilson, N., Mason, J.E., Morgan, D., and Gordon, M.N. (2004). Time-dependent reduction in Abeta levels after intracranial LPS administration in APP transgenic mice. Exp. Neurol. *190*, 245–253.

Hooijmans, C.R., Van der Zee, C.E., Dederen, P.J., Brouwer, K.M., Reijmer, Y.D., van Groen, T., Broersen, L.M., Lütjohann, D., Heerschap, A., and Kiliaan, A.J. (2009). DHA and cholesterol containing diets influence Alzheimer-like pathology, cognition and cerebral vasculature in APPswe/PS1dE9 mice. Neurobiol. Dis. *33*, 482–498.

Hsiao, K., Chapman, P., Nilsen, S., Eckman, C., Harigaya, Y., Younkin, S., Yang, F., and Cole, G. (1996). Correlative memory deficits, Abeta elevation, and amyloid plaques in transgenic mice. Science *274*, 99–102.

Imbimbo, B.P., Giardino, L., Sivilia, S., Giuliani, A., Gusciglio, M., Pietrini, V., Del Giudice, E., D'Arrigo, A., Leon, A., Villetti, G., and Calzà, L. (2010). CHF5074, a novel gamma-secretase modulator, restores hippocampal neurogenesis potential and reverses contextual memory deficit in a transgenic mouse model of Alzheimer's disease. J. Alzheimers Dis. *20*, 159–173.

Jankowsky, J.L., Slunt, H.H., Ratovitski, T., Jenkins, N.A., Copeland, N.G., and Borchelt, D.R. (2001). Co-expression of multiple transgenes in mouse CNS: a comparison of strategies. Biomol. Eng. *17*, 157–165.

Jankowsky, J.L., Fadale, D.J., Anderson, J., Xu, G.M., Gonzales, V., Jenkins, N.A., Copeland, N.G., Lee, M.K., Younkin, L.H., Wagner, S.L., et al. (2004). Mutant presenilins specifically elevate the levels of the 42 residue beta-amyloid peptide in vivo: evidence for augmentation of a 42-specific gamma secretase. Hum. Mol. Genet. *13*, 159–170.

Kanekiyo, T., Liu, C.C., Shinohara, M., Li, J., and Bu, G. (2012). LRP1 in brain vascular smooth muscle cells mediates local clearance of Alzheimer's amyloid-β. J. Neurosci. *32*, 16458–16465.

Korotzer, A.R., Pike, C.J., and Cotman, C.W. (1993). beta-Amyloid peptides induce degeneration of cultured rat microglia. Brain Res. *624*, 121–125.

Krabbe, G., Halle, A., Matyash, V., Rinnenthal, J.L., Eom, G.D., Bernhardt, U., Miller, K.R., Prokop, S., Kettenmann, H., and Heppner, F.L. (2013). Functional impairment of microglia coincides with Beta-amyloid deposition in mice with Alzheimer-like pathology. PLoS ONE *8*, e60921.

Kühn, R., Löhler, J., Rennick, D., Rajewsky, K., and Müller, W. (1993). Interleukin-10-deficient mice develop chronic enterocolitis. Cell *75*, 263–274.

Ledeboer, A., Brevé, J.J., Wierinckx, A., van der Jagt, S., Bristow, A.F., Leysen, J.E., Tilders, F.J., and Van Dam, A.M. (2002). Expression and regulation of interleukin-10 and interleukin-10 receptor in rat astroglial and microglial cells. Eur. J. Neurosci. *16*, 1175–1185.

Li, M.O., and Flavell, R.A. (2008). Contextual regulation of inflammation: a duet by transforming growth factor-beta and interleukin-10. Immunity *28*, 468–476.

Lio, D., Licastro, F., Scola, L., Chiappelli, M., Grimaldi, L.M., Crivello, A., Colonna-Romano, G., Candore, G., Franceschi, C., and Caruso, C. (2003). Interleukin-10 promoter polymorphism in sporadic Alzheimer's disease. Genes Immun. *4*, 234–238.

Loewenbrueck, K.F., Tigno-Aranjuez, J.T., Boehm, B.O., Lehmann, P.V., and Tary-Lehmann, M. (2010). Th1 responses to beta-amyloid in young humans convert to regulatory IL-10 responses in Down syndrome and Alzheimer's disease. Neurobiol. Aging *31*, 1732–1742.

Lopes, K.O., Sparks, D.L., and Streit, W.J. (2008). Microglial dystrophy in the aged and Alzheimer's disease brain is associated with ferritin immunoreactivity. Glia *56*, 1048–1060.

Ma, S.L., Tang, N.L., Lam, L.C., and Chiu, H.F. (2005). The association between promoter polymorphism of the interleukin-10 gene and Alzheimer's disease. Neurobiol. Aging *26*, 1005–1010.

Maezawa, I., Zimin, P.I., Wulff, H., and Jin, L.W. (2011). Amyloid-beta protein oligomer at low nanomolar concentrations activates microglia and induces microglial neurotoxicity. J. Biol. Chem. *286*, 3693–3706.

Mawuenyega, K.G., Sigurdson, W., Ovod, V., Munsell, L., Kasten, T., Morris, J.C., Yarasheski, K.E., and Bateman, R.J. (2010). Decreased clearance of CNS beta-amyloid in Alzheimer's disease. Science *330*, 1774.

McGeer, P.L., Akiyama, H., Itagaki, S., and McGeer, E.G. (1989). Activation of the classical complement pathway in brain tissue of Alzheimer patients. Neurosci. Lett. *107*, 341–346.

Meda, L., Cassatella, M.A., Szendrei, G.I., Otvos, L., Jr., Baron, P., Villalba, M., Ferrari, D., and Rossi, F. (1995). Activation of microglial cells by beta-amyloid protein and interferon-gamma. Nature *374*, 647–650.

Michelucci, A., Heurtaux, T., Grandbarbe, L., Morga, E., and Heuschling, P. (2009). Characterization of the microglial phenotype under specific pro-inflammatory and anti-inflammatory conditions: Effects of oligomeric and fibrillar amyloid-beta. J. Neuroimmunol. *210*, 3–12.

Miller, K.R., and Streit, W.J. (2007). The effects of aging, injury and disease on microglial function: a case for cellular senescence. Neuron Glia Biol. *3*, 245–253.

Mucke, L., and Selkoe, D.J. (2012). Neurotoxicity of amyloid β-protein: synaptic and network dysfunction. Cold Spring Harb Perspect Med *2*, a006338.

Murray, P.J. (2006). Understanding and exploiting the endogenous interleukin-10/STAT3-mediated anti-inflammatory response. Curr. Opin. Pharmacol. *6*, 379–386.

Nicoll, J.A., Wilkinson, D., Holmes, C., Steart, P., Markham, H., and Weller, R.O. (2003). Neuropathology of human Alzheimer disease after immunization with amyloid-beta peptide: a case report. Nat. Med. *9*, 448–452.

Nicoll, J.A., Barton, E., Boche, D., Neal, J.W., Ferrer, I., Thompson, P., Vlachouli, C., Wilkinson, D., Bayer, A., Games, D., et al. (2006). Abeta species removal after abeta42 immunization. J. Neuropathol. Exp. Neurol. *65*, 1040–1048.

O'Leary, T.P., and Brown, R.E. (2009). Visuo-spatial learning and memory deficits on the Barnes maze in the 16-month-old APPswe/PS1dE9 mouse model of Alzheimer's disease. Behav. Brain Res. *201*, 120–127.

Ramos, E.M., Lin, M.T., Larson, E.B., Maezawa, I., Tseng, L.H., Edwards, K.L., Schellenberg, G.D., Hansen, J.A., Kukull, W.A., and Jin, L.W. (2006). Tumor necrosis factor alpha and interleukin 10 promoter region polymorphisms and risk of late-onset Alzheimer disease. Arch. Neurol. *63*, 1165–1169.

Richard, K.L., Filali, M., Préfontaine, P., and Rivest, S. (2008). Toll-like receptor 2 acts as a natural innate immune receptor to clear amyloid beta 1-42 and delay the cognitive decline in a mouse model of Alzheimer's disease. J. Neurosci. *28*, 5784–5793.

Scassellati, C., Zanardini, R., Squitti, R., Bocchio-Chiavetto, L., Bonvicini, C., Binetti, G., Zanetti, O., Cassetta, E., and Gennarelli, M. (2004). Promoter haplotypes of interleukin-10 gene and sporadic Alzheimer's disease. Neurosci. Lett. *356*, 119–122.

Schenk, D., Barbour, R., Dunn, W., Gordon, G., Grajeda, H., Guido, T., Hu, K., Huang, J., Johnson-Wood, K., Khan, K., et al. (1999). Immunization with amyloid-beta attenuates Alzheimer-disease-like pathology in the PDAPP mouse. Nature *400*, 173–177.

Shaftel, S.S., Kyrkanides, S., Olschowka, J.A., Miller, J.N., Johnson, R.E., and O'Banion, M.K. (2007). Sustained hippocampal IL-1 beta overexpression mediates chronic neuroinflammation and ameliorates Alzheimer plaque pathology. J. Clin. Invest. *117*, 1595–1604.

Sjölander, J., Westermark, G.T., Renström, E., and Blom, A.M. (2012). Islet amyloid polypeptide triggers limited complement activation and binds complement inhibitor C4b-binding protein, which enhances fibril formation. J. Biol. Chem. *287*, 10824–10833.

Streit, W.J., Braak, H., Xue, Q.S., and Bechmann, I. (2009). Dystrophic (senescent) rather than activated microglial cells are associated with tau pathology

and likely precede neurodegeneration in Alzheimer's disease. Acta Neuropathol. *118*, 475–485.

Strle, K., Zhou, J.H., Shen, W.H., Broussard, S.R., Johnson, R.W., Freund, G.G., Dantzer, R., and Kelley, K.W. (2001). Interleukin-10 in the brain. Crit. Rev. Immunol. *21*, 427–449.

Tampellini, D., Capetillo-Zarate, E., Dumont, M., Huang, Z., Yu, F., Lin, M.T., and Gouras, G.K. (2010). Effects of synaptic modulation on beta-amyloid, synaptophysin, and memory performance in Alzheimer's disease transgenic mice. J. Neurosci. *30*, 14299–14304.

Tan, J., Town, T., Paris, D., Mori, T., Suo, Z., Crawford, F., Mattson, M.P., Flavell, R.A., and Mullan, M. (1999). Microglial activation resulting from CD40-CD40L interaction after beta-amyloid stimulation. Science *286*, 2352–2355.

Tan, J., Town, T., Mori, T., Wu, Y., Saxe, M., Crawford, F., and Mullan, M. (2000). CD45 opposes beta-amyloid peptide-induced microglial activation via inhibition of p44/42 mitogen-activated protein kinase. J. Neurosci. *20*, 7587–7594.

Tan, J., Town, T., Crawford, F., Mori, T., DelleDonne, A., Crescentini, R., Obregon, D., Flavell, R.A., and Mullan, M.J. (2002). Role of CD40 ligand in amyloidosis in transgenic Alzheimer's mice. Nat. Neurosci. *5*, 1288–1293.

Town, T., Nikolic, V., and Tan, J. (2005). The microglial "activation" continuum: from innate to adaptive responses. J. Neuroinflammation *2*, 24.

Town, T., Laouar, Y., Pittenger, C., Mori, T., Szekely, C.A., Tan, J., Duman, R.S., and Flavell, R.A. (2008). Blocking TGF-beta-Smad2/3 innate immune signaling mitigates Alzheimer-like pathology. Nat. Med. *14*, 681–687.

Townsend, K.P., Town, T., Mori, T., Lue, L.F., Shytle, D., Sanberg, P.R., Morgan, D., Fernandez, F., Flavell, R.A., and Tan, J. (2005). CD40 signaling regulates innate and adaptive activation of microglia in response to amyloid beta-peptide. Eur. J. Immunol. *35*, 901–910.

Trouw, L.A., Nielsen, H.M., Minthon, L., Londos, E., Landberg, G., Veerhuis, R., Janciauskiene, S., and Blom, A.M. (2008). C4b-binding protein in Alzheimer's disease: binding to Abeta1-42 and to dead cells. Mol. Immunol. *45*, 3649–3660.

Ubhi, K., Peng, K., Lessig, S., Estrella, J., Adame, A., Galasko, D., Salmon, D.P., Hansen, L.A., Kawas, C.H., and Masliah, E. (2010). Neuropathology of dementia with Lewy bodies in advanced age: a comparison with Alzheimer disease. Neurosci. Lett. *485*, 222–227.

Vural, P., Değirmencioğlu, S., Parildar-Karpuzoğlu, H., Doğru-Abbasoğlu, S., Hanagasi, H.A., Karadağ, B., Gürvit, H., Emre, M., and Uysal, M. (2009). The combinations of TNFalpha-308 and IL-6 -174 or IL-10 -1082 genes polymorphisms suggest an association with susceptibility to sporadic late-onset Alzheimer's disease. Acta Neurol. Scand. *120*, 396–401.

Webster, S.J., Bachstetter, A.D., and Van Eldik, L.J. (2013). Comprehensive behavioral characterization of an APP/PS-1 double knock-in mouse model of Alzheimer's disease. Alzheimers Res Ther *5*, 28.

Weitz, T.M., and Town, T. (2012). Microglia in Alzheimer's Disease: It's All About Context. Int. J. Alzheimers Dis. *2012*, 314185.

Wilcock, D.M., Munireddy, S.K., Rosenthal, A., Ugen, K.E., Gordon, M.N., and Morgan, D. (2004). Microglial activation facilitates Abeta plaque removal following intracranial anti-Abeta antibody administration. Neurobiol. Dis. *15*, 11–20.

Williams, L.M., Ricchetti, G., Sarma, U., Smallie, T., and Foxwell, B.M. (2004). Interleukin-10 suppression of myeloid cell activation—a continuing puzzle. Immunology *113*, 281–292.

Wyss-Coray, T., and Mucke, L. (2002). Inflammation in neurodegenerative disease—a double-edged sword. Neuron *35*, 419–432.

Wyss-Coray, T., Lin, C., Yan, F., Yu, G.Q., Rohde, M., McConlogue, L., Masliah, E., and Mucke, L. (2001). TGF-beta1 promotes microglial amyloid-beta clearance and reduces plaque burden in transgenic mice. Nat. Med. *7*, 612–618.

Zhang, B., Gaiteri, C., Bodea, L.G., Wang, Z., McElwee, J., Podtelezhnikov, A.A., Zhang, C., Xie, T., Tran, L., Dobrin, R., et al. (2013). Integrated systems approach identifies genetic nodes and networks in late-onset Alzheimer's disease. Cell *153*, 707–720.

Zhu, Y., Hou, H., Rezai-Zadeh, K., Giunta, B., Ruscin, A., Gemma, C., Jin, J., Dragicevic, N., Bradshaw, P., Rasool, S., et al. (2011). CD45 deficiency drives amyloid-β peptide oligomers and neuronal loss in Alzheimer's disease mice. J. Neurosci. *31*, 1355–1365.

Zotova, E., Holmes, C., Johnston, D., Neal, J.W., Nicoll, J.A., and Boche, D. (2011). Microglial alterations in human Alzheimer's disease following Aβ42 immunization. Neuropathol. Appl. Neurobiol. *37*, 513–524.